# Critical properties and phase separation in lattice Boltzmann fluid mixtures

by

Nicos S. Martys
Building and Fire Research Laboratory
National Institute of Standards and Technology
Gaithersburg, MD 20899 USA

and

Jack F. Douglas
Material Science Engineering Laboratory
National Institute of Standards and Technology
Gaithersburg, MD 20899 USA

Reprinted from Physical Review E, Vol. 63, 1-18, 2001.




NIST
National Institute of Standards and Technology
Technology Administration, U.S. Department of Commerce

# Critical properties and phase separation in lattice Boltzmann fluid mixtures

Nicos S. Martys[1] and Jack F. Douglas[2]
[1]*Building Materials Division, Building and Fire Research Laboratory, National Institute of Standards and Technology, Gaithersburg, Maryland 20899*
[2]*Polymers Division, Material Science Engineering Laboratory, National Institute of Standards and Technology, Gaithersburg, Maryland 20899*
(Received 4 May 2000; published 27 February 2001)

Basic equilibrium properties of lattice Boltzmann (LB) fluid mixtures (coexistence curve, surface tension, interfacial profile, correlation length) are calculated to characterize the critical phenomena occurring in these model liquids and to establish a reduced variable description allowing a comparison with real fluid mixtures. We observe mean-field critical exponents and amplitudes so that the LB model may be useful for modeling high molecular weight polymer blends and other fluid mixtures approximated over a wide temperature range by mean-field theory. We also briefly consider phase separation under quiescent and shearing conditions and point out the strong influence of interacting boundaries on the qualitative form of the late-stage phase-separation morphology.

DOI: 10.1103/PhysRevE.63.031205 PACS number(s): 47.11.+j, 05.20.Dd, 02.70.−c

## I. INTRODUCTION

In many applications involving materials processing and development, it is necessary to understand and control the morphology of multiphase fluid mixtures and particulate dispersions subject to a complex flow history. These applications often involve free liquid-air boundaries that can respond to flow and phase-separation processes, solid boundaries that can be preferentially wet by certain liquid components, thin-film geometries, complex solid substrate geometries, and high Reynolds number flows in which fluid inertia is important. The development of computational methods of sufficient flexibility and generality to treat such realistic fluid dynamics problems is a basic theoretical challenge.

The lattice Boltzmann (LB) method and other related computational methods based on cellular-automata ideas (e.g., lattice gas) [1] have emerged as powerful tools for modeling complex fluid dynamics problems. These methods are developing rapidly in response to recent theoretical advances and the availability of resources for large-scale computation. Applications of LB to modeling high Reynolds flow [1], the dynamics of fluid phase separation [2,3], and multicomponent fluid flow in porous media [4–6] have proven the potential of LB as a general purpose computational scheme for modeling complex fluid dynamics problems. Many of these exploratory studies have emphasized the development of the LB methodology and have not considered a direct comparison to the properties of real liquids. Therefore, basic characteristics of these computational models of liquids are still largely unknown. In this paper, we characterize the type of critical phenomena observed in two LB models of multicomponent liquids. The first model, due to Shan and Chen [2], modifies the Boltzmann equilibrium distribution to account for fluid-fluid interactions. The second approach, considered in the present paper, incorporates the forcing between two fluids directly into the body-forcing term of the Boltzmann equation [7]. In Appendix A, we show how the second method is related to a density-gradient expansion of a BBGKY collision operator [8–10], which should facilitate comparison with the Cahn-Hilliard theory of phase separation [11–16] and the Ginzburg-Landau theory of critical phenomena [17,18].

We calculate basic equilibrium properties (coexistence curve, interfacial width and correlation length, surface tension) and express our results in terms of a reduced variables description that allows comparison with real fluid measurements. Asymmetry in the mass and volume of the fluid components is considered in this comparison since this property is characteristic of real liquids. The effect of flow and interacting boundaries on the phase separation process is briefly explored to identify some basic phenomena of experimental interest.

## II. BRIEF REVIEW OF LATTICE BOLTZMANN MODEL OF FLUID PHASE SEPARATION

The LB method of modeling fluid dynamics is actually a family of models with varying degrees of faithfulness to the properties of real liquids. These methods are currently in a state of evolution as the models become better understood and corrected for various deficiencies. In the present work, we utilize two LB models of complex fluids. The first and primarily studied method in this paper was proposed by Shan and Chen [2,5]. It is particularly simple in form and adaptable to complex flow conditions such as the presence of solid-fluid and air-fluid boundaries. For comparison, a second approach is studied [7] that directly incorporates the fluid/fluid interaction into a body-force term. This approach removes second-order contributions with respect to the forcing (see below). The physical basis of such an approach is further described in Appendix A. A third approach, not studied in this paper, is due to Yeomans *et al.* [3,16] and is strongly rooted in the Cahn-Hilliard model of binary mixtures [12–16]. A major criticism of this approach is the lack of Galilean invariance, but recent work suggests that the errors involved can be controlled in the description of the phase separation of fluids in the absence of shear [16]. It

remains to be seen whether these higher-order effects cause problems under conditions of fluid flow. All of these models, however, are not strictly energy conserving, which should be important under conditions of deep quenches and high rates of flow. Recent work [10] has introduced a framework for overcoming this technical problem and allows for systematic improvements of the LB calculation of fluid properties. In the present paper, we focus on isothermal flows and will examine the effect of energy conservation on the two-phase region of LB fluid mixtures in a future work.

We now present a brief description of the LB methods used in this study. A considerable computational advantage in modeling the fluid is obtained by restricting the particle positions to the sites of a lattice. The LB method extends the standard ''quasicrystalline'' fluid model [19–22] of classical statistical mechanics by specifying the particle velocity distribution at each particle position so that *both* equilibrium and dynamical properties of the fluid can be calculated. Macroscopic variables such as density and fluid velocity are obtained by taking suitable moments of the velocity distribution function. The velocity distribution function, $n_a^i(\mathbf{x},t)$, where the superscript $i$ labels the fluid component and the subscript $a$ indicates the velocity direction, is the number density of particles at node $\mathbf{x}$, time $t$ with velocity $\mathbf{e}_a$, where $a=1,\ldots,b$. In this study, the particle velocities are represented in terms of a basis set defined on a cubic lattice. The velocity vectors are directed towards points that are nearest and next-nearest neighbors about a central lattice site and are in units of the lattice spacing divided by the time step. In the literature, this lattice is called a D3Q19 lattice, where the 19 corresponds to the basis set size, $b=19$ [23]. Time is counted in discrete time steps, and the fluid particles can collide with each other as they move under applied forces (surface tension, applied shear, etc.). The directions of the particle velocities are discretized in such a way that the isotropy of the pressure tensor and other properties are preserved [1]. The discretization of the time and spatial coordinates greatly reduces the information required to specify the fluid dynamics, thus extending the scale of the system that can be modeled by a given computational resource. This is the computational virtue of a lattice formulation. The price is that care must be taken to avoid artifacts that arise from the lattice model.

Macroscopic quantities such as density, $\rho^i(\mathbf{x},t)$, and fluid velocity, $\mathbf{u}^i$, of each fluid component, $i$, are obtained by the following moment sums:

$$\rho^i(\mathbf{x},t)=m^i n^i(\mathbf{x},t)=m^i\sum_a n_a^i(\mathbf{x},t) \tag{1}$$

and

$$\mathbf{u}^i(\mathbf{x},t)=\frac{\sum_a n_a^i(\mathbf{x},t)\mathbf{e}_a}{n^i(\mathbf{x},t)}, \tag{2}$$

where $m^i$ is the molecular mass of the $i$th component. While the distribution function is defined only over a discrete set of velocities, the actual macroscopic velocity field of the fluid is nearly continuous.

The time evolution of the particle velocity distribution function satisfies the following LB equation:

$$n_a^i(\mathbf{x}+\mathbf{e}_a,t+1)-n_a^i(\mathbf{x},t)=\Omega_a^i(\mathbf{x},t), \tag{3}$$

where $\Omega_a^i$ is the collision operator representing the rate of change of the particle distribution due to collisions. The collision operator is greatly simplified by use of the single time relaxation approximation [23,24],

$$\Omega_a^i(\mathbf{x},t)=-\frac{1}{\tau_i}[n_a^i(\mathbf{x},t)-n_a^{i(\mathrm{eq})}(\mathbf{x},t)], \tag{4}$$

where $n_a^{i(\mathrm{eq})}(\mathbf{x},t)$ is the equilibrium distribution at $(\mathbf{x},t)$ and $\tau_i$ is the relaxation time that controls the rate of approach to equilibrium. The equilibrium distribution can be represented in the following form for particles of each type [23]:

$$n_a^{i(\mathrm{eq})}(\mathbf{x})=t_a n^i(\mathbf{x})[\tfrac{3}{2}(1-d_o^i)+3\mathbf{e}_a\cdot\mathbf{v}+\tfrac{3}{2}(3\mathbf{e}_a\mathbf{e}_a:\mathbf{vv}-\mathbf{v}^2)], \tag{5}$$

$$n_{19}^{i(\mathrm{eq})}(\mathbf{x})=t_{19}n^i(\mathbf{x})[3d_o-\tfrac{3}{2}\mathbf{v}^2], \tag{6}$$

where

$$\mathbf{v}=\frac{\sum_i^S m^i\sum_a n_a^i\mathbf{e}_a/\tau_i}{\sum_i^S m^i n^i(\mathbf{x})/\tau_i}, \tag{7}$$

and the weights are $t_a=\frac{1}{36}$ for $1\leqslant a\leqslant 12$, $t_a=\frac{1}{36}$ for $13\leqslant a\leqslant 18$, and $t_{19}=\frac{1}{3}$. The parameter $d_o^i$ can be related by self-consistency to an effective temperature, $T$, by the following moment of the equilibrium distribution:

$$T(\mathbf{x},t)=\frac{\sum_i m^i\sum_a n_a^{i(\mathrm{eq})}(\mathbf{x},t)(\mathbf{e}_a-\mathbf{v})^2}{3\sum_i n^i(\mathbf{x},t)}. \tag{8}$$

In order that both fluid components have the same temperature, $d_o^i$ may be defined by the relation $d_o^i=1-2(T/m^i)$, where we choose units here such that Boltzmann's constant $k_B$ equals 1.

It has been shown that the above formalism leads to a velocity field that is a solution of the Navier-Stokes [24] equation with the kinematic viscosity $\nu$ [2,5],

$$\nu=c^2\frac{\sum_i^S c_i\tau_i-\frac{1}{2}}{6}, \tag{9}$$

where $c_i$ is the concentration of each component and the lattice constant $c=\sqrt{2}$ for this model.

### A. Fluid interaction

An interaction force $\mathbf{F}^i$ for each fluid is needed to drive the phase-separation process. We use a simple interaction, suggested by Shan and Chen (the physical basis of this forcing is given in Appendix A), that depends on the density of each fluid:

$$\mathbf{F}^i = -n^i(\mathbf{x}) \sum_{i'}^{S} \sum_{a} G^a_{ii'} n^{i'}(\mathbf{x}+\mathbf{e}_a)\mathbf{e}_a , \tag{10}$$

where $G^a_{ii'}=2G$, $G$, and 0 for the cases $|\mathbf{e}^a|=1$, $|\mathbf{e}^a|=\sqrt{2}$, and, $i=i'$, respectively. $G$ is a coupling constant controlling the interaction strength. This term is analogous to a nearest-neighbor interaction in lattice models of interacting fluids. The forcing term has been shown to drive the phase separation and to produce an interfacial surface tension effect consistent with the Laplace law [5], which states that there is a pressure drop proportional to the local curvature at the interface boundary between two fluids.

In the LB model of Shan and Chen, phase separation takes place when the mutual diffusivity of the binary mixture becomes negative, providing a condition determining the critical coupling $G_c$ for phase separation. An analytical expression for the mutual diffusivity has been determined [25]. For a viscosity matched binary mixture in which the particle masses are also matched (''symmetric fluid mixture''), phase separation occurs when the critical coupling equals

$$G_c = \frac{T}{48} \frac{-c_1 n^1 - c_2 n^2 + \sqrt{(c_1 n^1 + c_2 n^2)^2 + 8 n^1 n^2}}{n^1 n^2}. \tag{11}$$

It is not ordinarily possible to exactly calculate the critical coupling for phase separation in three-dimensional liquids, and this condition for the critical coupling, $G_c$, is evidently a clue to the nature of the phase-separation process. Since the LB method neglects thermal fluctuations that renormalize the critical coupling constant $G$, this method is a *mean-field model* of fluid mixtures. This observation, which has basic ramifications for the applicability of the model in comparison with real fluid mixtures, is established numerically in the next section, where the critical properties are examined to establish the nature of the model.

Once the forcing is described, it must be properly incorporated into a LB model. Shan-Chen introduced the forcing by modifying the equilibrium velocity $\mathbf{v}$ [2]:

$$n^i(\mathbf{x})\mathbf{v}'(\mathbf{x}) = n^i \mathbf{v}(\mathbf{x}) + \tau_i \frac{\mathbf{F}^i}{\rho^i}, \tag{12}$$

where $\mathbf{v}'$ is the new velocity used in Eqs. (5) and (6). This approach introduces a momentum transfer between fluids that preserves momentum globally. The main criticism of the Shan-Chen model is that when shifting the velocity in the equilibrium distribution, additional corrections in the pressure tensor will appear that are of order $F^2$.

Instead of shifting the velocity in the equilibrium distribution as in the Shan-Chen model, the forcing between two fluids can be directly included in the body-force term of the Boltzmann equation. In the continuum Boltzmann equation, the body-force term is written $B^i = \mathbf{F}^i/\rho^i \cdot \nabla_e n^i(\mathbf{x},\mathbf{e})$, where $\mathbf{F}^i/\rho^i$ is an acceleration field due to a body force. An expression of this body-force term, to second order in Hermite polynomials [7], in the discrete velocity space of the D3Q19 lattice is given by

$$B^i_a = -3 t_a n^i(\mathbf{x}) \left[ (\mathbf{e_a} - \mathbf{v}) \cdot \frac{\mathbf{F}^i}{\rho^i} + 3(\mathbf{e_a}\cdot\mathbf{v}) \left( \mathbf{e_a} \cdot \frac{\mathbf{F}^i}{\rho^i} \right) \right]. \tag{13}$$

One can think of this acceleration field as being due to a ''mean field'' produced by the surrounding molecules (see Appendix A). The main difference between this approach and the Shan-Chen model is that it avoids terms of order $F^2$ that result from the shift of the velocity in the equilibrium distribution, so that the linearity of the forcing is preserved. The effect of this modification of the LB model is investigated below.

Finally, Eq. (10) can be modified to mimic an interaction between the solid surface and fluid [5]. Here $n^{i'}(\mathbf{x}+\mathbf{e_a})$ is given the value 1 or 0 depending on whether $\mathbf{x}+\mathbf{e}_a$ resides on a point in the solid or fluid, respectively, and the value of $G^a_{ii'}$ is then set to allow the solid to attract a fluid (wetting) or to repulse a fluid (nonwetting).

## III. EQUILIBRIUM CRITICAL PHENOMENA IN A LB FLUID MIXTURE

An understanding of the equilibrium critical phenomena of fluid mixtures is necessary for modeling the flow of multiphase materials. This understanding is not only required for estimating phase stability and the type of phase-separation process (droplet growth or bicontinuous fluid pattern formation [12–16]), but also for transport properties (collective diffusion, self-diffusion, viscosity) that depend sensitively on the nature of the critical phenomena occurring in the liquid. This is natural given the existence of order-parameter (fluid composition) fluctuations that cause a mode coupling between momentum and mass transport processes [26–32]. Our first task in developing the LB model for these many practical applications (involving phase-separating fluid mixtures under flow conditions) is to establish the type of equilibrium critical phenomena exhibited by this model fluid mixture. While the LB models do have hydrodynamic interactions, they do not treat hydrodynamic couplings associated with non-mean-field contributions to the mode-coupling between compositional and velocity fluctuations [26–29]. The theory is thus a mean-field theory also in the sense of fluid dynamics, and the implications of this constraint require further investigation.

## IV. COEXISTENCE CURVE FOR LB MIXTURE

For a sufficiently large fluid interaction coupling, $G$, the LB mixtures of components $A$ and $B$ phase-separate into liquids having coexisting compositions $\phi_A$ and $\phi_B$ at equilibrium. The composition variables $\phi_A$ and $\phi_B$ denote the relative volume fractions of the two fluid components. These

dimensionless concentration units are normalized so that $\phi_A+\phi_B=1$. Compressibility effects on the fluid mixture can be treated through the addition of an additional vacancy component $\phi_c$ such that $\phi_A+\phi_B+\phi_c=1$, as in equilibrium lattice model calculations of compressible mixtures [33], but this complication is not considered in the present paper.

Increasing the LB coupling $G$ makes the coexisting compositions more enriched in the pure components and thus has the same qualitative effect as lowering the temperature in systems exhibiting an ''upper critical temperature'' type phase separation (i.e., phase separation upon cooling). The parameter $G$ thus plays a role similar to the binary interaction parameter $\varepsilon$ in the lattice model of fluid mixtures [19–22,34],

$$\varepsilon=\varepsilon_{AB}-(\varepsilon_{AA}+\varepsilon_{BB})/2, \tag{14}$$

where $\varepsilon_{AB}$ and $\varepsilon_{AA},\varepsilon_{BB}$ denote the mutual and self-nearest-neighbor interactions of the fluid components. $G$ is also analogous to the well depth parameter $\varepsilon_{\mathrm{LJ}}$ in off-lattice models of phase separation based on Lenard-Jones or related potentials [35]. In all these models, it is the relative value of the ''interaction strength'' $(G,\varepsilon,\varepsilon_{\mathrm{LJ}})$ to the temperature that is the dimensionless coupling constant defining the tendency toward phase separation. For example, the dimensionless interaction in the lattice model of fluid mixtures is conventionally defined as [19–22,34]

$$\chi=q\varepsilon/k_bT, \tag{15}$$

where $q$ and $k_bT$ denote the lattice coordination number and thermal energy, respectively. The inclusion of the $q$ factor is made to weight the number of possible nearest-neighbor interactions. In magnetic phase transitions, we have the same form of dimensionless couplings as Eq. (13), where $\varepsilon$ is replaced by the ''exchange interaction'' $J$ modeling the short-range magnetic interparticle interaction [18,36]. From these measures of interaction, we see that lowering the temperature has basically the same effect as increasing the interaction coupling $(\varepsilon,\varepsilon_{\mathrm{LJ}})$ for the usual case where ordering occurs upon cooling. Phase separation in the LB liquid also occurs when the temperature is lowered with $G$ fixed, and we similarly define a dimensionless coupling constant,

$$\chi_G\equiv G/k_bT. \tag{16}$$

A reduced variable temperature $\tau$ may then be defined from the interaction coupling constant, $\chi_G$,

$$\tau_G\equiv\frac{|T/G-T/G_c|}{T/G_c} \tag{17}$$

for our simulation performed at fixed temperature $T$ and variable $G$. For a particular fluid mixture it is natural to fix $G$ and to vary $T$ so that the reduced temperature variable is defined as

$$\tau'_G\equiv\frac{|T/G-T_c/G|}{T_c/G}, \tag{18}$$

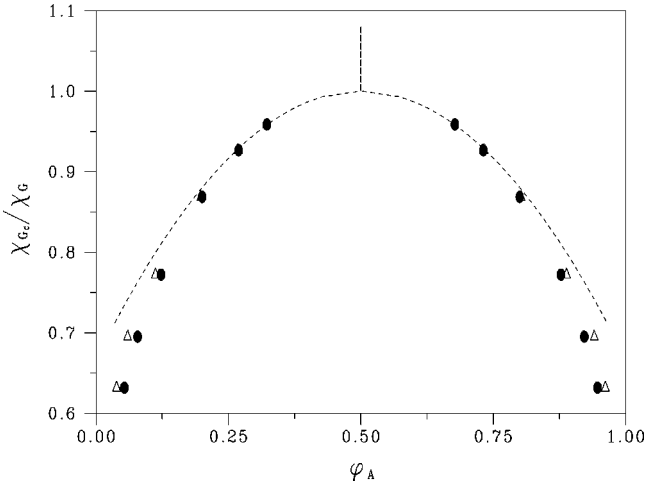


FIG. 1. Phase diagram of LB fluid mixture. Normalized coupling $\chi_{G_c}/\chi_G$ versus the composition $\phi_A$ of fluid $A$. The solid circles represent data from the Shan-Chen model and the triangles represent data from the body-forcing model. $\chi_{G_c}/\chi_G$ also corresponds to the temperature ratio $T/T_c$.

where $T_c$ is the critical temperature for a fixed value of $G$. The absolute value definition in Eqs. (17) and (18) ensures that the reduced temperature variable is positive for notational simplicity, but this requires that we must carefully distinguish between the one-phase and two-phase regions. All of the computations of the present paper are performed in the two-phase region.

In Fig. 1, we present our results for the coexistence curve of a symmetric LB fluid mixture (both mass and viscosity ratios of fluid components are equal). The $y$ axis denotes the ratio of critical dimensionless coupling to the dimensionless coupling, $\chi_{G_c}/\chi_G$, defined in Eq. (16) and the $x$ axis denotes the composition $\phi_A$ of the $A$ fluid. We observe that the critical composition $\phi_{c,A}$ of the $A$ component equals $\phi_c=\frac{1}{2}$ (a ''symmetric mixture''), as required by the symmetry of exchange of the fluid components. This exchange symmetry is well known in lattice models of fluid phase separation [37–41]. The composition difference $\Delta\phi=\phi_A^{(1)}-\phi_A^{(2)}$ between the coexisting phases defines an order parameter for the fluid phase-separation process. The relation of $\Delta\phi$ to the reduced temperature is indicative of the type of critical phenomena (''universality class'') under discussion. In a mean-field model of fluid phase separation, $\Delta\phi$ is described by the general relation [17,18,34]

$$\Delta\phi=2B\tau^{\beta},\quad \tau=(T-T_c)/T_c,\quad T\approx T_c, \tag{19}$$

where the order-parameter exponent $\beta$ and critical amplitude $B$ for a symmetric incompressible fluid mixture equal [34]

$$B=\sqrt{3}/2,\quad \beta=\tfrac{1}{2}. \tag{20}$$

The dashed line in Fig. 1 is the predicted value. Our data are consistent with the mean-field prediction as $\tau_G\to 0$. Note that the Shan-Chen model deviates more from the mean-field prediction than does the simple body-forcing model. In general, it was found that the linear body forcing was somewhat

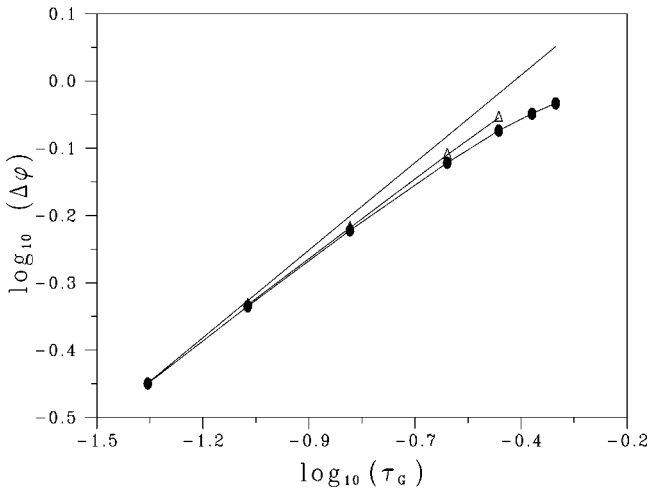


FIG. 2. Order parameter $\Delta\phi$ versus quench depth parameter $\tau_G$.

more stable. The mean-field theory prediction [Eq. (19)] is further examined in Fig. 2, where we plot $\log_{10}(\Delta\phi)$ versus $\log_{10}(\tau_G)$ for the lattice data shown in Fig. 1. It is apparent that a power-law scaling of $\Delta\phi$ on $\tau_G$ is observed over an appreciable temperature range. The solid line denotes the prediction of Eq. (19) with no free parameters, where $\tau$ is equated with $\tau_G$. Note that the critical temperature is not adjustable in this comparison, in contrast to most simulations and experiments in which this quantity is not known exactly. Of course, the solution of the two-dimensional Ising spin model and its lattice-gas analog is an exception to this general situation [17,18]. Sengers gives an excellent review of the critical properties of fluids and fluid mixtures that provides much further information about mean-field and non-mean-field critical properties and the ''crossover'' between these property scaling regimes [42].

Figures 1 and 2 not only verify that the phase-separation process in LB fluids is described well by mean-field theory, but they also establish the utility of our definition of reduced temperature scale, $\tau_G$, which is required for other applications involving LB fluid mixtures. For example, we can quantify the quench depth of our phase-separation measurements by specifying the $\tau_G$ value. These simulations can be compared to experiments on real fluids at the corresponding $\tau$ value. Quantitative agreement with the properties of real liquids can only be expected for liquids that can be modeled by mean-field theory over a broad temperature range (see the discussion below). This identification between computational and real fluids is generally restricted to a temperature range over which mean-field critical behavior is exhibited to a good approximation. Strictly speaking, no real fluids are described by mean-field critical behavior, but for many fluids the approximation should be reasonable provided $\tau$ is sufficiently far from the critical point defined by the limit $\tau \rightarrow 0^+$. The Ginzburg criterion defines the temperature range over which mean-field theory is a reasonable approximation [33,43–50].

Real fluid mixtures are characterized by differences in the molecular shapes and volumes of the fluid molecules and asymmetries in the intermolecular interaction potentials that destroy the symmetry of exchange between the fluid components [38–40]. This symmetry breaking is evident in the shape of the coexistence curve. The graph of $\Delta\phi$ versus $\tau$ becomes ''skewed'' so that the critical composition $\phi_c$ no longer equals $\frac{1}{2}$ [38–40]. The molecular asymmetry effect is particularly evident in polymer fluid mixtures where the ratio of the molecular weights and the backbone chain structure can be adjusted to ''tune'' the asymmetry of the coexistence curve [21,22,34,51]. The asymmetry becomes extreme in the case of high molecular weight polymers dissolved in low molecular weight solvents where $\phi_{A,c}$ of the high molecular weight component approaches zero with increasing molecular weight [21,52]. It is also possible to modify the molecular weights of a blend to achieve an almost perfect symmetry as in Fig. 1 [53]. This symmetry is not usually observed in fluid mixtures or in single-component fluid phase transitions, although the degree of asymmetry is usually modest in comparison with polymer solutions.

The breaking of the particle exchange symmetry arising from differences in molecular shape, rigidity, mass, and other molecular parameters is difficult to describe in a mesoscale fluid model of phase separation. We can obtain a simple model of this symmetry-breaking phenomenon, however, by considering the idealized Flory-Huggins (FH) mean-field model of polymer blend phase separation [21], which accounts minimally for the molecular mass asymmetry of the fluid components (actually, the model accounts for a volume asymmetry since this incompressible polymer blend model assumes all lattice sites are occupied and have equal density). Notably, the FH model completely ignores polymer topology, monomer asymmetry, polydispersity in the size and monomer-monomer interactions, and other factors that surely influence polymer blend stability, but the mass ratio in the FH model does provide a parameter that allows the asymmetry of the coexistence curve to be ''tuned'' to fit observations on real blends. (The recently developed lattice cluster mean-field theory generalizes the FH model by incorporating leading-order correlations associated with chemical connectivity and monomer structure [33].) We first consider the case in which the particle masses are ''asymmetric'' in the LB fluid model in the same spirit of approximation. Figure 3 shows the coexistence curve for a LB fluid mixture having a mass ratio $\delta_M = M_A/M_B = 3$, where the concentration difference $\Delta\phi$ between the coexisting phases is given in *number density* concentration units rather than the volume fraction units of Fig. 1. We examine the scaling of $\Delta\phi$ on the quench depth parameter $\tau_G$ in Fig. 4, where we find a mean-field scaling exponent $\frac{1}{2}$ as in Figs. 1 and 2 and a shift of the critical coupling to the value $G_c = 0.0135$. The asymmetry of the coexistence curve is quantified by calculating the dependence of the average composition $\overline{\phi_A} = (\phi_A^{(1)} + \phi_A^{(2)})/2$ in the coexistence curve shown in Fig. 3, where $\phi_A^{(1)}$ and $\phi_A^{(2)}$ are compositions of the coexisting phases. According to the ''law of rectilinear diameter'' of Cailletet and Mathias [54], $\overline{\phi}$ is linear function of $\tau$. This linearity is found to a good approximation in the asymmetric fluid phase-separation coexistence curve shown in Fig. 3. The average composition $\phi_A$ is shown in Fig. 5, where the line denotes the rectilinear diameter fit,

$$\overline{\phi_A} = \phi_{A,c} + A\tau_G, \tag{21}$$

where $A$ is a constant, $A=0.11$, and $\overline{\phi_A}$ and $\phi_{A,c}$ are given in number fraction units. This type of plot is an effective way to determine the critical composition of an asymmetric fluid mixture [55]. Fluctuation corrections to mean-field theory can lead to deviations from Eq. (21) in real fluids that are important near the critical point [56].

We can also break the symmetry of interparticle exchange and thus distort the shape of the phase boundary by varying the relative volumes of the fluid particles (see Appendix B). In Fig. 6, we show the phase boundary calculated for a range of values of $\lambda$, the ratio of the volumes of components $A$ and $B$, $\lambda = V_A/V_B$. We assume spherically shaped particles so that $\lambda$ scales as the cube of the ratio of the particle radii, $\lambda = (R_A/R_B)^3$. By convention, we take the $A$ fluid component to have the largest molecular volume. Increasing the particle size asymmetry strongly increases the asymmetry of the phase boundary, in qualitative agreement with the Flory-Huggins theory of polymer phase separation [21,22,34]. Note that the data in Fig. 6 are given in volume fraction units. The simple Flory mean-field treatment of the Flory-Huggins lattice model indicates that $\phi_c = 1/[1+\lambda^{1/2}]$, where $\lambda$ is the relative chain molecular volume (see below). The true critical composition seems to be approximated reasonably well by a similar expression, $\phi_c = 1/[1+\lambda]$, and the arrows in the figure show the result in comparison with the data. We note that the phase diagrams of micelle and protein solutions, where there is a large asymmetry in the size of the phase-separating species, tend to be asymmetric as in Fig. 6 [57].

In applications of the LB model to real measurements, we can phenomenologically adjust the relative mass (and thus the critical composition in Figs. 3 and 4) or relative particle volume $\lambda$ and identify the LB order-parameter variable [$\phi_A$ (number density) or volume fraction units, respectively] with the experimentally determined order-parameter concentration unit. While this is generally an approximation, we expect it to provide a reasonable mimic of the critical properties of asymmetric fluid mixtures as in previous experience with the FH model [58].

### A. Interfacial composition profile and correlation length

The interface between phase-separated liquids becomes diffuse near a critical point where the interfacial tension becomes relatively low. The width of this interface can be quantified through the determination of the composition interfacial profile $\phi_A(z)$, which measures the local composition along a coordinate, $z$, normal to an interface between the coexisting phases.

An interface in near-critical fluid mixtures can be probed by optical reflectivity [59–61] or ellipsometry [62–64] to determine its width, but accurate measurements of composition gradients across the interface are difficult. Direct measurement of $\phi_A(z)$ has recently become possible in thin films by neutron reflection [65,66], but the broadening of these profiles by capillary waves and surface wetting effects complicates the interpretation of those measurements so that it is hard to quantitatively evaluate theory in this important area [67–70]. The LB model allows the determination of $\phi_A(z)$ for an ideal mean-field theory fluid. Some insight into the fluctuation contribution to $\phi_A(z)$ can be obtained by comparing these calculations to Monte Carlo calculations of $\phi_A(z)$ [69,70]. An important property that derives from the determination of $\phi_A(z)$ is the correlation length $\xi^-$ in the two-phase region, which governs the average width of the interface (see below). This definition of the correlation length is more involved in asymmetric fluid mixtures since the composition profile, $\phi_A(z)$, is asymmetric about the center ($z=0$) of the fluid interface.

Figure 7 shows an equilibrium interfacial composition profile $\phi_A(z)$ for a symmetric LB mixture having a quench depth in the two-phase region, $\tau_G = 0.1$. The numerically determined profile $\phi_A(z)$ is fit well by the mean-field theory prediction [11,63,70–72],

$$\phi_A(z) = \overline{\phi} + (\Delta\phi/2)\tanh(z/w) \tag{22}$$

for all $\tau_G$ considered in our paper. The dependence of the interfacial width $w$ on reduced temperature $\tau_G$ is indicated in Fig. 8. The mean-field correlation length $\xi^-$ of the fluid mixture in the two-phase mixture is related to $w$ by [64,70,72]

$$2\xi^- \equiv w \tag{23}$$

so that the determination $\phi_A(z)$ affords a means of determining the basic property $\xi^-$. A fit to the $w$ data nearest the critical point in Fig. 8 gives

$$\xi^- = (0.96 \pm 0.05)\,\tau_G^{-\nu}, \tag{24}$$

where the mean-field value of the critical exponent $\nu = \frac{1}{2}$ is assumed. Far away from the critical point, where $\tau_G \sim O(1)$, the correlation length becomes comparable to the lattice spacing, as in Monte Carlo simulation of phase separation in small molecule liquids [70]. The lattice spacing in the LB model should be interpreted as being comparable to the average range of the interparticle interaction potential. This scale is typically comparable to the average molecular dimensions of the molecule involved [73], and for polymers this scale can be fairly large [74]. Particle clustering can also increase the magnitude of this scale in small molecule liquids [75].

In a mean-field model of phase separation, the correlation length $\xi$ has the same singular dependence on reduced temperature, $\tau_G$, in the one- and two-phase regions ($\xi^+$ and $\xi^-$, respectively) [76],

$$\xi = \xi_o^- \tau_G^{-1/2}, \quad \xi = \xi_o^+ \tau_G^{-1/2}, \tag{25}$$

but the correlation length amplitudes $\xi_o^+, \xi_o^-$ are related by a constant ratio in mean-field theory [76],

$$\xi_o^+/\xi_o^- = 2^{1/2}. \tag{26}$$

This ''universal'' ratio is closer to 2 in real fluid mixtures exhibiting Ising-type criticality [77,78]. The discrepancy between Eq. (26) and measurement is illustrative of the large

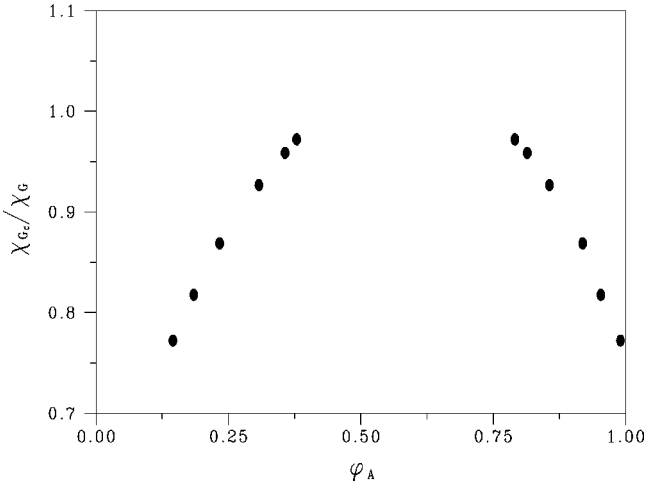


FIG. 3. Phase diagram of an asymmetric LB fluid mixture.

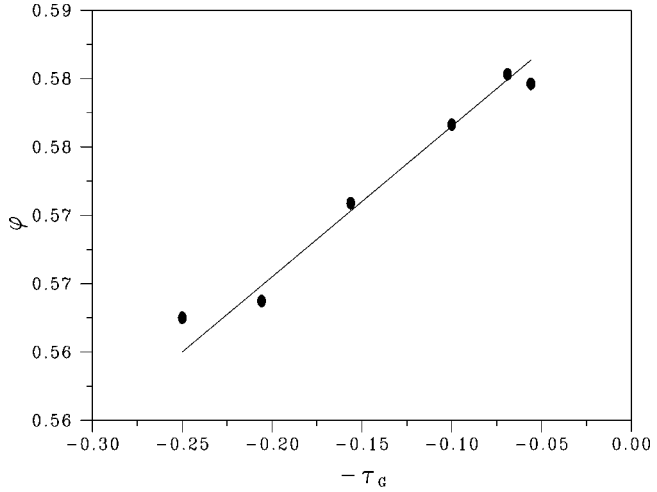


FIG. 5. Rectilinear diameter $\phi=(\phi_A+\phi_B)/2$ versus quench depth $\tau_G$.

property changes that critical fluctuations can induce. Moreover, the critical temperature, in three dimensions, can be shifted from its mean-field value by as much as 25% by fluctuations, so that the interaction parameters must be treated as phenomenological parameters in comparison to experiments in order to ''absorb'' these discrepancies [34].

The interfacial composition profile $\phi_A(z)$ of asymmetric fluid mixtures composed of mixtures of dissimilar molecules is also asymmetric [79]. We briefly illustrate this effect in Fig. 9 for a fluid having a mass ratio $\delta_M=3$ and a quench depth $\tau_G=0.1$. Again, we present our concentration data for the asymmetric fluid in terms of number density units to simply realize the effect of fluid asymmetry [80]. While the equilibrium profile may appear to be like the tanh profile [Eq. (22)] found in the symmetric case, we could not obtain a good fit to this function. A good empirical description of this profile is found by first taking a derivative of the profile in Figure 9 to find its inflection point and by then fitting to a tanh profile on *each side* of the inflection point [65,81]. Fig. 9 shows a fit to the data where the characteristic widths $w_L=5.75$ and $w_R=5.0$ correspond to the left and right sides of the inflection point. The average $\overline{w}=(w_L+w_R)/2$ provides a good measure of the average interfacial width. We plan to discuss the properties of the LB model with a molecular volume asymmetry further in a separate publication so that this case is not discussed here. In all the discussion below, we restrict ourselves to $\lambda=1$.

It has sometimes been reported that two correlation lengths exist in the two-phase region of fluid mixtures having asymmetric coexistence curves [75]. These measurements are made by performing light or neutron scattering on coexisting phases in macroscopically phase-separated samples. The scale of the composition fluctuations appears to occur at different scales in the $\phi_A$-rich and $\phi_A$-poor coexisting phases [75]. Apparently, the measurement process can give rise to unequal weighting in the different phases to the two sides of the $\phi_A(z)$ profile, leading to different $\xi^-$ estimates. Although such measurements provide some insight into the

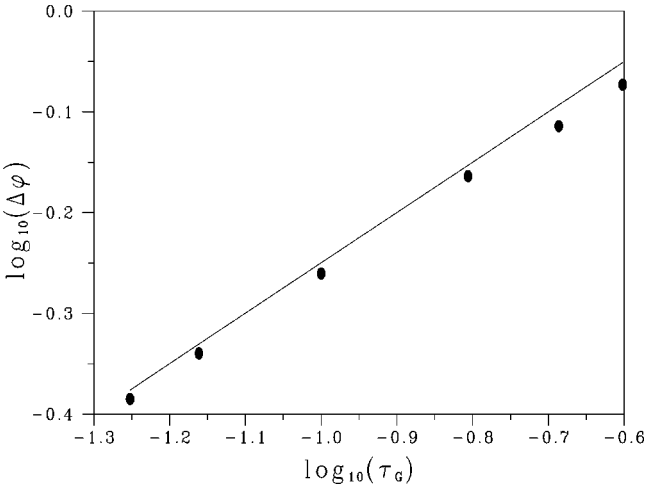


FIG. 4. Order parameter $\Delta\phi$ vs quench depth parameter $\tau_G$ for an asymmetric LB mixture.

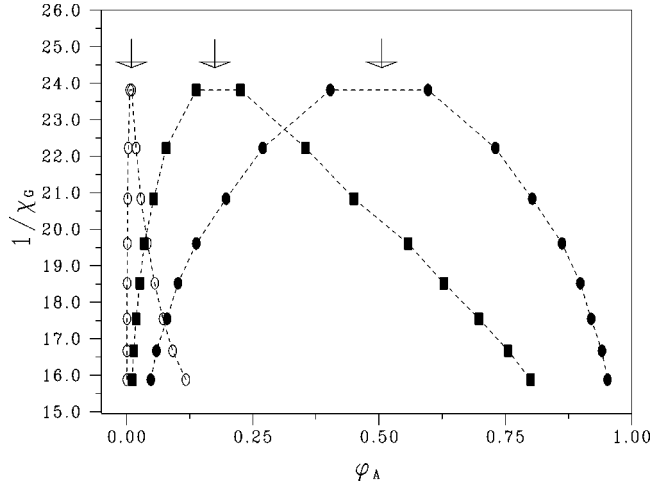


FIG. 6. Influence of particle size on phase boundary asymmetry. $\lambda=1.0$ (filled circles), 4.63 (filled squares), and 125.0 (open circles). Dashed lines are included to help guide the eye.

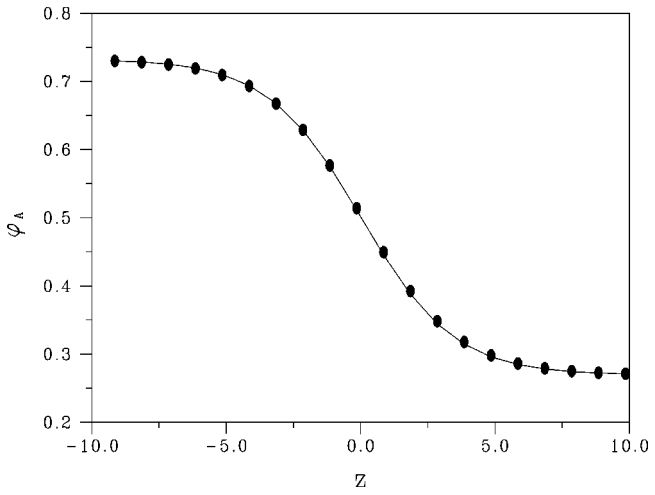


FIG. 7. Interface composition profile $\phi_A$ for a quench depth $\tau_G=0.08$. $z$ is in the direction normal to the center of the fluid interface. Solid line is fit to Eq. (22).

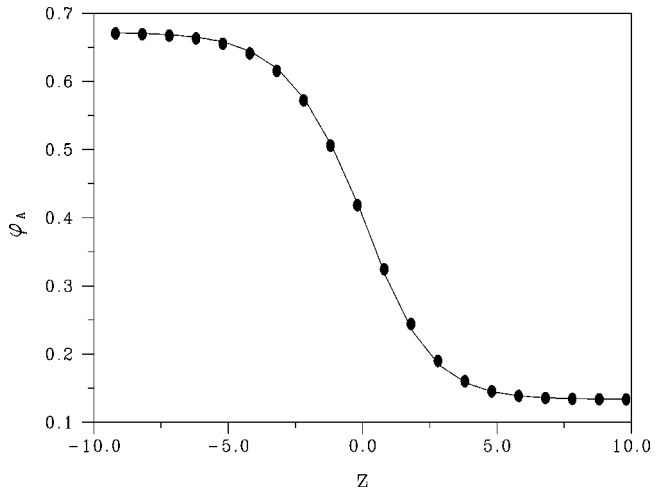


FIG. 9. The interfacial composition (number density) profile $\phi_A(z)$ of an asymmetric fluid mixture having a mass ratio $\delta_M=3$ and quench depth $\tau_G=0.08$.

asymmetry of the $\phi_A(z)$ profile, they should not be interpreted as implying the existence of two distinct correlation lengths in the two-phase region.

### B. Interfacial tension

Interfacial tension measurements provide a direct means of probing the interaction between fluids. This property is crucial in an industrial context for controlling the size and phase stability of mechanically dispersed droplets and other transient structures formed in the course of phase separation. In principle, the interfacial tension, $\sigma$, provides a conceptually simple means of determining the reduced temperature variable $\tau=(T-T_c)/T_c$ needed to characterize the phase stability of fluid mixtures, but experimental complications [82,83] (e.g., high viscosity in polymeric systems) have limited somewhat the application of this method to the critical phenomena of fluid mixtures. Part of the difficulty is the need for a more predictive theory of interfacial tension on which reliable thermodynamic interaction ($\chi$ or $G$) measurements can be based. Recently, there has been great effort in modeling the interfacial tension of polymeric blends by Monte Carlo simulation methods as a guide to improving analytic theory in this important area of technological application [69,70].

We calculate the LB interfacial tension $\sigma$ through an integration of the interfacial composition profile,

$$\sigma=\int (P_{zz}-\tfrac{1}{2}[P_{xx}+P_{yy}])dz, \tag{27}$$

where $P_{zz}$ and $\frac{1}{2}[P_{xx}+P_{yy}]$ are the normal and tangential parts of the pressure tensor, respectively. The numerical values of the interfacial tension for the symmetric LB fluid mixture, shown in Fig. 10, are consistent with a power law,

$$\sigma=\sigma_o\tau_G^{1.5}, \quad \sigma_0\approx 4.2 \tag{28}$$

over a broad temperature range. The exponent 1.5 is an established result for the interfacial tension in mean-field

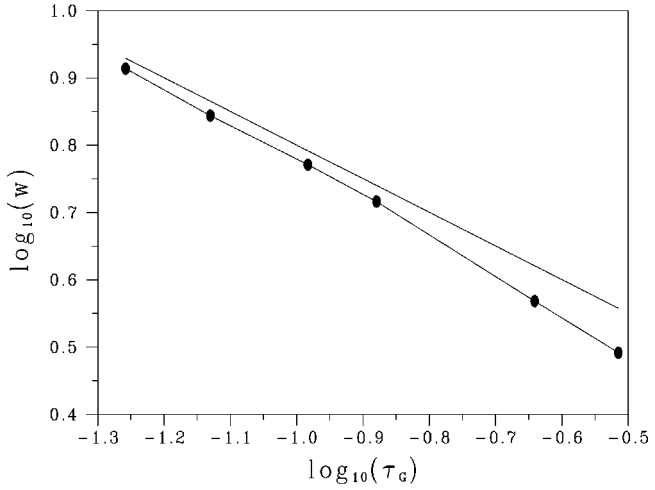


FIG. 8. Interfacial width $w$ as a function of the reduced interaction $\tau_G$.

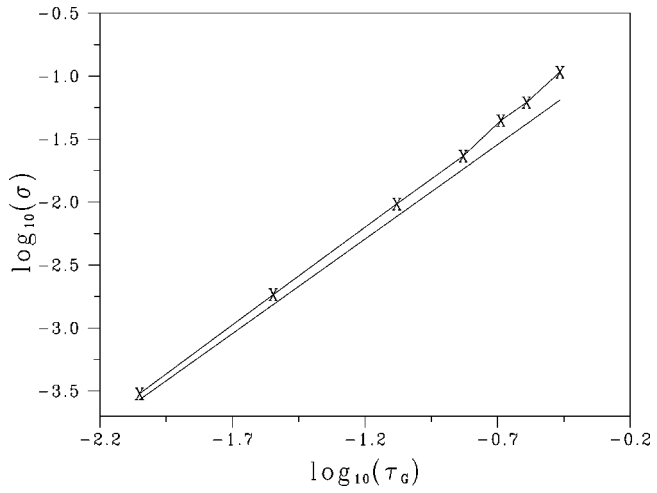


FIG. 10. Interfacial tension versus quench depth, $\tau_G$.

theory [12,70], and is found to agree reasonably well with observations outside the critical region [84–86]. Fluctuation effects modify the exponent to a value $\approx 1.25$ [87]. This fluctuation-modified exponent is often found to be quite accurate near the critical point for phase separation [77,78]. The amplitude of the interfacial tension, $\sigma_0$, is a nonuniversal quantity that depends on the interparticle potential range, interparticle spacing, and molar volume of the liquid. Further discussion of the origin of interfacial tension in the LB model is given in Appendix A.

## V. COMPARISON OF THE LB FLUID MIXTURE MODEL TO POLYMER BLENDS

It is apparent from the examination of the LB mixture model above that the critical properties of this fluid are described by mean-field theory and that the critical exponents predicted by this model are inconsistent with those measured for many real mixtures. This limits, of course, the comparison of LB model calculations to certain qualitative trends in the equilibrium properties of near-critical fluid mixtures. (The theory should become more reliable, however, away from the critical point.) Such inconsistencies can also be expected for certain dynamic properties near the critical point. For example, the shear viscosity of a near critical Ising-type fluid mixture diverges near the critical point while no divergence occurs in a model mean-field mixture [88]. Mode-coupling effects due to compositional flucuations have an even larger effect on the collective diffusion coefficient [30,31]. Although mean-field models of fluid mixtures are idealized, there is a class of real liquids whose behavior approaches this ideal type critical behavior. The phase separation of polymer blends in the theoretical limit of infinite molecular weight of the homopolymer components has been argued [45,46] to be described by mean-field theory, so that the phase separation of high molecular weight blends should be reasonably approximated by this idealized model. Monte Carlo calculations support these theoretical arguments, although the chain length must generally be rather high for this approximation to apply [89,90]. There have also been recent reports of apparent mean-field critical behavior in fluid mixtures with salts [90] and in ionic fluid mixtures [91].

It is common practice in polymer science to fit the critical properties of polymer blends to the Flory-Huggins (FH) mean-field lattice model of phase separation where all inaccuracies of the modeling (monomer structure, chain architecture, compressibility, . . .) are absorbed into the phenomenological ''$\chi$ parameter'' in Eq. (16) [92]. A virtue of the FH lattice model is that it often allows the prediction of qualitative trends in the scattering properties of polymer blends. We can retain this advantage and avoid the conceptual pitfalls of interpreting $\chi$ too literally as a ''molecular'' parameter by establishing a formal correspondence between the parameters of this model and the LB fluid mixture model.

In the FH model of polymer blend phase separation, the reduced temperature variable is [46,92]

$$\tau_{\mathrm{FH}} = |\chi - \chi_c|/\chi = |T_c - T|/T_c , \tag{29}$$

where the critical interaction $\chi_c$ is defined by the condition

$$\chi_c = (2N_A\phi_c)^{-1} + [2N_B(1-\phi_c)]^{-1} \tag{30}$$

and $N_A$ and $N_B$ are homopolymer polymerization indices. *Symmetric* blends are defined by the idealized condition $N_A = N_B = N$ so that $\phi_c = \frac{1}{2}$ and $\chi_c = 2/N$. The critical composition $\phi_c$ of the blend no longer equals $\frac{1}{2}$ when the blends are not symmetric ($N_A \geqslant N_B$) [21,46,74],

$$\phi_c = \frac{N_B^{1/2}}{N_A^{1/2} + N_B^{1/2}}. \tag{31}$$

As mentioned above, the incorporation of asymmetry into the LB model requires adjusting the mass asymmetry or volume asymmetry to give a variation in the critical composition. We can then *mimic* the asymmetric phase of the phase boundary of polymer blends by varying the mass asymmetry $\delta_M$ or $\lambda$ and formally replacing $\tau_G$ by $\tau_{\mathrm{FH}}$.

The correlation length $\xi$ of the FH model in conjunction with the random-phase approximation [46,74] yields a scaling relation for $\xi$ in the two-phase region for a symmetric blend

$$\xi^- = \xi_0^- \, {\tau_{\mathrm{FH}}}^{-1/2}, \quad \xi_0^- = R_g/\sqrt{6}, \tag{32}$$

where $R_g$ is the chain radius of gyration. We see from a comparison of Eqs. (32) to the LB expression Eq. (23) that the lattice spacing in a coarse-grained model of polymer blends must be large since the lattice spacing is on the order of $R_g$. This implies that the lattice spacing must be taken to depend on chain molecular weight in comparison with measurements. Moreover, the predictions of the LB model must be considered with caution when physically relevant scales in physical problems become smaller than this coarse-graining scale (lattice spacing) of the LB lattice model. This limitation is natural since the LB model is a mesoscopic description of a fluid rather than a microscopic model.

There are a number of points to be drawn from our discussion of polymer blend critical properties in comparison with the LB model of fluid phase separation.

(i) Polymer blends are reasonable candidates for comparison with the LB mixture model.

(ii) The mean-field model gives rise to universal scaling relationships that should allow fixing the parameters of the LB model according to the blend molecular characteristics. This gives some insight into the qualitative variation of the LB parameters with the variation of molecular structure.

(iii) Comparison of the LB model with parameters fixed by the FH model with Monte Carlo calculations of the lattice model of polymer blends should provide some insight into the mean-field approximation in the case of properties not tractable using analytic mean-field theory. For example, we can compare LB calculations of the interfacial tension to Monte Carlo calculations for polymer blends that avoid the mean-field approximation.

(iv) Fixing the LB model parameters through ''matching'' to the FH model then allows a comparison with dynamical properties (transport coefficients) and processes (phase separation, wetting, dewetting) of blends calculated using the mean-field approximation.

(v) The expression of the results of measurements in terms of general and universal scaling relations (when they exist) offers advantages to representations involving the phenomenological $\chi$ interaction parameter. Expressions between large-scale observable properties deduced from mean-field theory often have greater applicability than expressions between observables and temperature-like variables such as $\chi$ and $\tau$.

## VI. SOME ILLUSTRATIVE CALCULATIONS OF PHASE SEPARATION WITH AND WITHOUT SHEAR AND THE INFLUENCE OF INTERACTION BOUNDARIES ON PHASE SEPARATION

Now that we have established the type of critical phenomena exhibited by the LB model of fluid mixtures and a reduced variable description for some of the basic thermodynamic properties of this model fluid mixture, we can apply the LB model to the description of phase separation under a wide range of conditions. In this section, we will illustrate some phenomena we have investigated in connection with recent measurements.

The comparison of nonequilibrium phenomena such as fluid phase separation to LB model calculations requires the introduction of a dimensionless time unit that is common between the experimental and computational fluids. For fluid phase separation, it is conventional to express reduced time in terms of the mutual diffusion coefficient $D_m$ and the correlation length, $\xi^-$ [93–95]. We thus divide our computational time $t$ by the average initial rate of phase separation, $t_{\rm ps}=2(\xi^-)^2/|D_m|$, deduced from Cahn-Hilliard theory [11,93–95]. The mutual diffusion coefficient obtained for the Shan-Chen model studied in this paper for a viscosity matched binary mixture is given by

$$D_m=\tau T\left[\frac{1-G'^2n^1n^2}{1+G'(c_1n^2+c_2n^1)}-\frac{1}{2}\right], \tag{33}$$

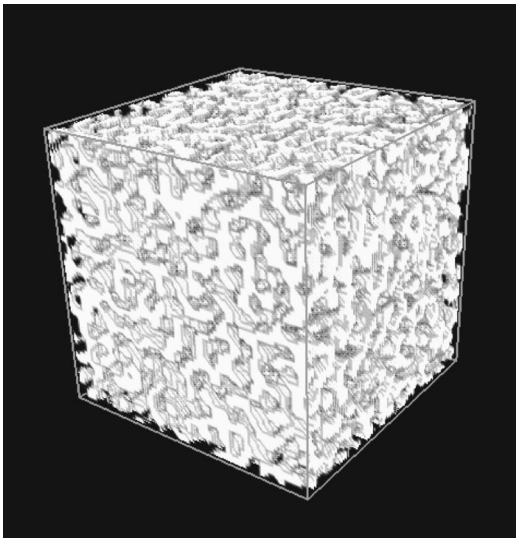

FIG. 11. ''Spinodal'' phase separation morphology in critical composition (50-50 relative composition) fluid mixture. The quench depth equals $\tau_G=0.537$ and $\bar{t}=3.6$.

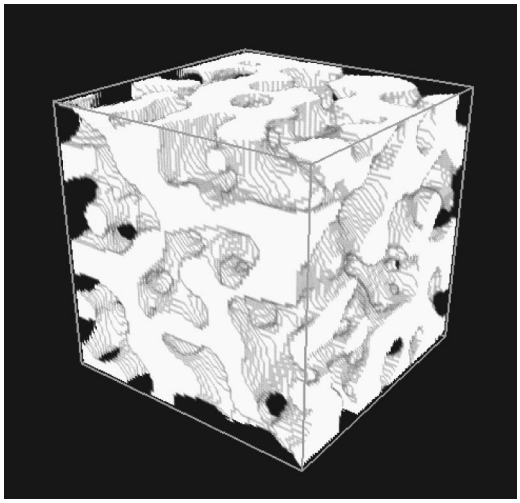

FIG. 12. Spinodal phase separation in critical composition fluid mixture. Note the similarity of the structure in Fig. 12 to Fig. 11, apart from scale. This observation reflects the existence of dynamic scaling in the mixture coarsening. The quench depth equals $\tau_G=0.537$ and $\bar{t}=17.8$.

where $G'=12G/T$. All times below are reported in the dimensionless time $\bar{t}=t/t_{\rm ps}$ in our discussion of the LB model of fluid phase separation. Results are presented from simulations corresponding to a sytem size of $80^3$ in units of lattice spacing cubed.

### A. Phase separation without shear

In Fig. 11, we illustrate the case of a critical composition ($\phi_A=\frac{1}{2}, m_A=m_B$). The value of the ''quench depth'' equals $\tau_G=0.537$ and the reduced time, $\bar{t}=3.6$. Periodic boundary conditions are employed in this LB calculation to minimize wall effects. Figure 12 shows separation after a later time, $\bar{t}=17.8$. The pattern is similar in geometric form to Fig. 11, but the characteristic scale of the pattern is larger after longer

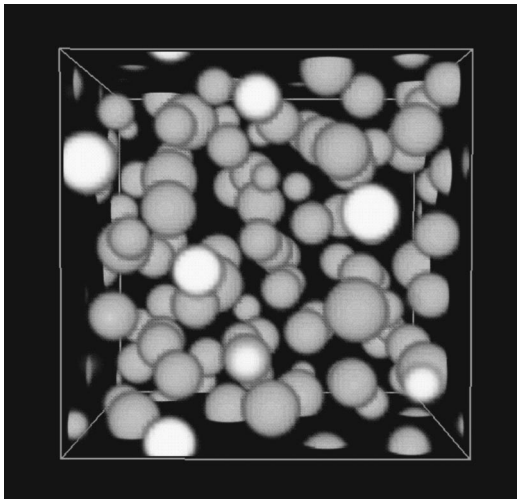

FIG. 13. Off-critical (10-90 relative composition) phase separation showing droplet formation and coarsening. The quench depth $\tau_G=0.133$ and $\bar{t}=8.4$.

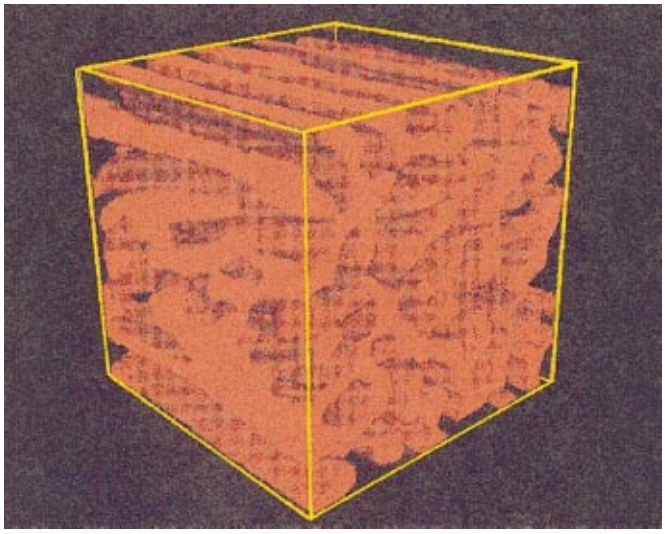

FIG. 14. (Color) Sheared critical composition blend. The ''string'' structures are observed along shearing planes where the strings are oriented in the direction of the fluid flow. The quench depth $\tau_G = 0.537$, $\bar{t} = 8.5$, and $\dot{\gamma} t_p = 0.18$.

times, geometrically illustrating the notion of *dynamic similarity* in the phase-separation coarsening process. A study of the time dependence of the growth of the phase separation shows that the pattern scale grows slowly in the early stage of the phase-separation process, as the local composition builds up to its coexisting composition value (one of the coexisting phases, $\phi_B$, has been rendered transparent in Fig. 11). At a later stage of phase separation, the pattern scale growth is roughly linear in time [96,97]. Other LB studies have recently focused on modeling the kinetics of phase separation, so we do not dwell on this well known phenom-

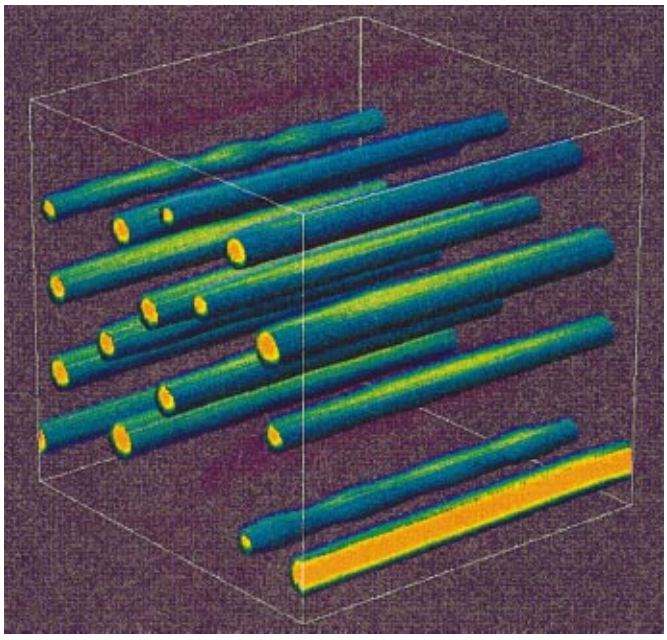

FIG. 15. (Color) Early-stage off-critical (15-85) phase separation under shear. For Figs. 15–17, orange represents the regions of high localized phase fraction of fluid $A$ ($\phi_A = 0.15$). The green regions represent the transition to a high localized phase fraction of fluid $B$, $\phi_B = 0.85$. Note the incipient Taylor-Tomitaka instability in some of the fluid ''strings.'' The quench depth $\tau_G = 0.287$, $\bar{t} = 16.4$, and the dimensionless shear rate $\dot{\gamma} t_p = 0.56$.

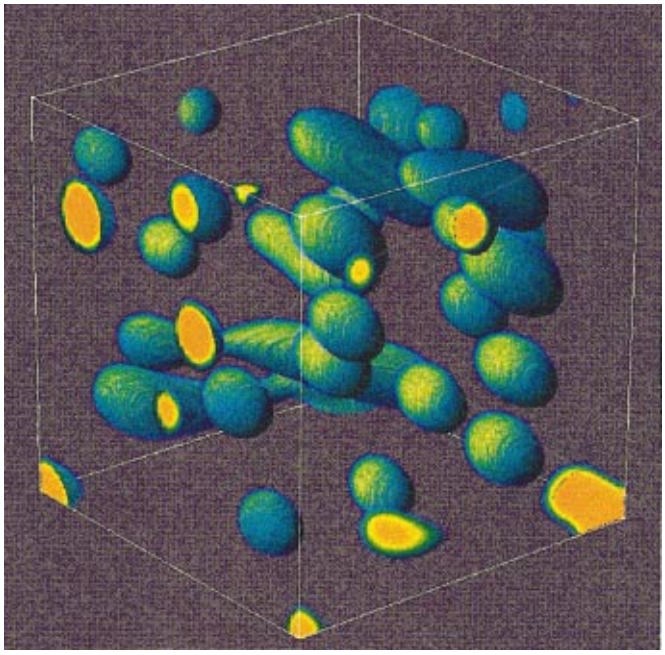

FIG. 16. (Color) Intermediate stage off-critical (15-85) phase separation ($\bar{t} = 27.6$). Droplets form after the fluid threads in Fig. 15 break up by the Taylor-Tomotika instability.

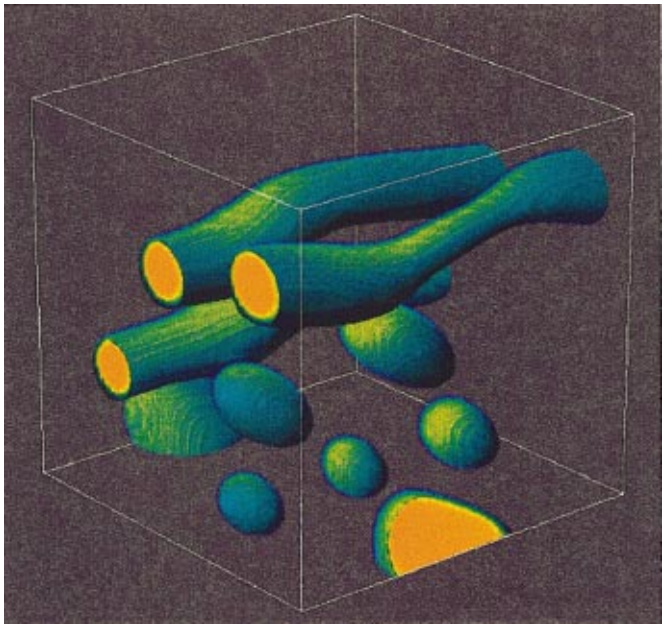

FIG. 17. (Color) Late-stage off-critical (15-85) phase separation ($\bar{t} = 56.8$). Droplets shown in Fig. 15 reconnect into stringlike structures that appear to persist and coarsen in cross-sectional dimension with time. The strings in Fig. 17 are contrasted with the ''stringslike'' structures near the mixture surface in Fig. 14, representative of a critical composition fluid mixture.

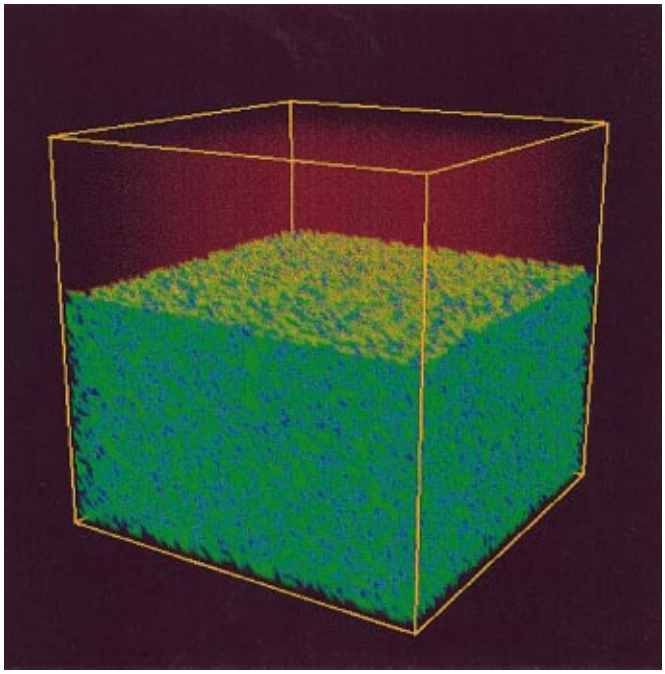

FIG. 18. (Color) Initial density of three phase systems to undergo surface-driven phase separation. The blue and green regions correspond to the location of the two-phase mixture. A third phase, lying above, is rendered as the translucent red region. The quench depth $\tau_G = 0.7$.

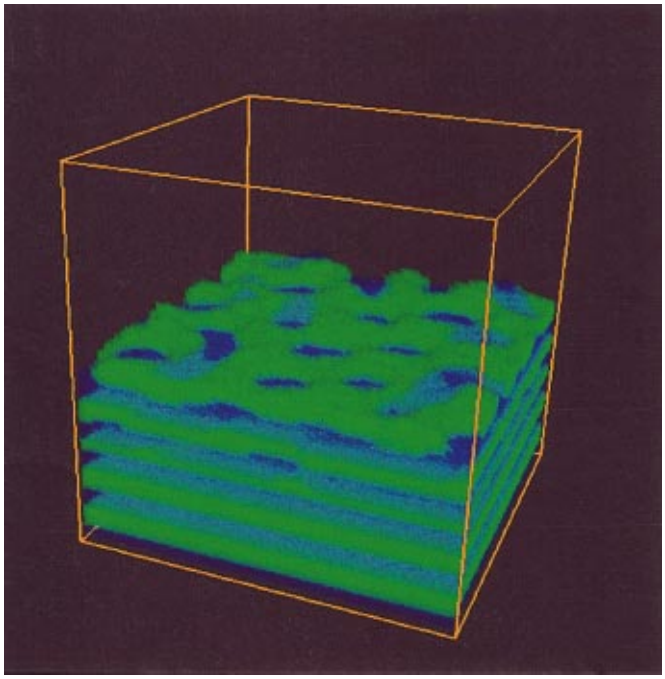

FIG. 20. (Color) Phase separation of a fluid mixture between interacting solid and air boundaries. This image indicates the development of an instability that disrupts the layers in late-stage phase separation. The reduced time equals $\bar{t} = 1.6$.

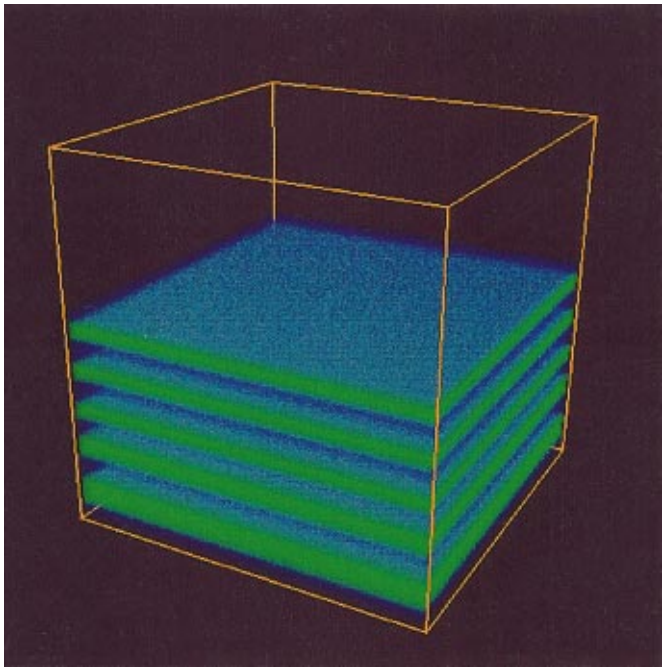

FIG. 19. (Color) ''Surface-directed'' phase separation. Phase separation of a fluid mixture between interacting solid and air boundaries. The layered morphology corresponds to ''surface-directed spinodal decomposition.'' This stage of the phase separation corresponds to $\bar{t} = 1.0$.

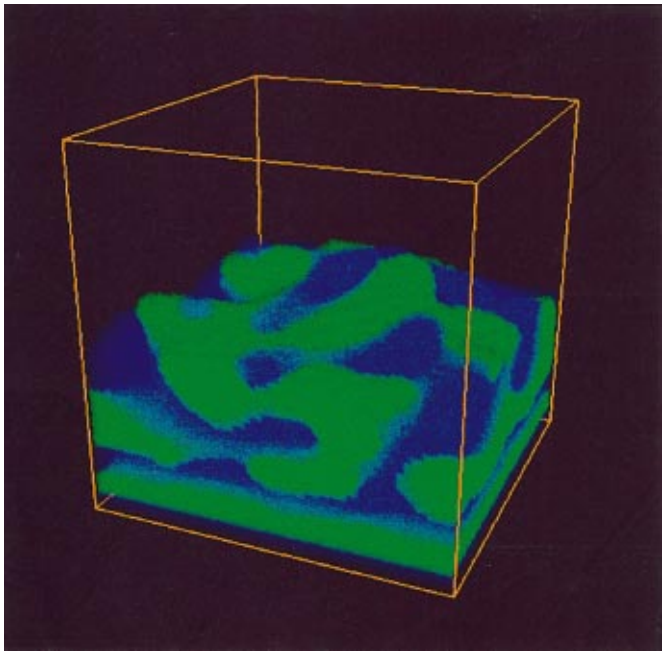

FIG. 21. (Color) ''Disrupted'' surface-directed phase separation. The disruption effect of ''pinching'' of the layers allows for further coarsening and leads to a collapse of the layered structure shown in Figs. 19 and 20. The reduced time equals $\bar{t} = 4.0$.

enon in the present paper [11,97–100]. We next illustrate the *qualitative* change in the phase-separation morphology that occurs under off-critical conditions. Figure 13 shows the phase-separation morphology for a quench depth, $\tau_G = 0.133$. The rendered composition $\phi_A$ is taken to have the off-critical value $\phi_A = 0.1$. The phase separation then occurs through droplet formation rather than the formation of a bicontinuous ''spinodal'' phase-separation pattern. At a later time, we observe the droplets to coarsen by coalescence in a normal manner for off-critical fluids [101]. In future work, we plan to explore the conditions (e.g., quench depth, viscosity mismatch, etc.) that determine the crossover between the droplet and bicontinuous phase-separation patterns observed in the early stages of phase separation. Even this basic aspect of fluid phase separation remains poorly understood so that materials scientists must rely on engineering correlations [102].

### B. Phase separation under a steady shearing flow

We next illustrate a nontrivial application of the LB method to a situation in which fluid flow is crucially important. Figure 14 shows the phase separation of a critical composition ($\phi_A = \phi_B$, $M_A = M_B$) blend for the same quench as shown in Fig. 11. The upper and lower boundaries in the figure are energetically ''neutral'' (neither fluid preferentially wets the surface.) A hydrodynamic ''stick'' boundary condition is imposed at the walls. The top and bottom walls move at velocities $u_w$ and $-u_w$ such that the dimensionless shear rate equals $\dot{\gamma} t_{\mathrm{ps}} = (2u_w/d) t_{\mathrm{ps}} = 0.18$, where $d$ is the spacing between the walls. The boundary condition is periodic in the direction parallel to the translating planes. We observe in the top view that the phase-separation pattern appears to have a ''stringlike'' form at the boundary, but that the structure within the film is actually more complicated. The phase separation in the plane perpendicular to the flow is remarkably undisturbed by the flow and closely resembles a *two-dimensional* phase-separation pattern in the absence of shear. As time proceeds, the ''penetration depth'' of the surface-induced ''stringlike'' structures in Fig. 14 increases and the phase-separation morphology ultimately coarsens to a state where the fluid interface lies perpendicular to the shearing planes and parallel to the flow direction. The surface-induced ''structuring'' of the blend morphology would be accentuated in the early stages of phase separation if one of the blend components had a preferential attraction to the shearing boundaries. This surface interaction evidently has a symmetry-breaking effect, since the fluid interface was found to lie *parallel* to the interface of the shearing boundaries at long times, when the boundary interaction was modified in this fashion. This illustrative calculation shows that the surface interaction can have a large influence on the ultimate alignment of a phase-separated fluid under shear. It is also apparent that the interpretation of optical and scattering data on sheared phase-separated fluids is complicated by the existence of gradients in the composition and structure of the fluid. Clearly, these observations warrant a thorough investigation of the many parameters that seem relevant to the phenomena (quench depth, surface energy, viscosity, molecular weight mismatch, roughness of shearing surface, steady and oscillatory shear, etc.). We note that many experiments have recently reported ''stringlike'' structures in sheared phase-separating fluids using both light scattering and optical microscopy techniques [48,103,104], and ''stringlike'' structures have also been reported in two-dimensional LB phase-separation simulations [105]. The case of two dimensions is somewhat special, however, since the Taylor-Tomotika [106] instability is suppressed in two dimensions [107].

An illustration of phase-separation in an off-critical blend under steady shear also provides important insights into the kinds of phase-separation morphologies that can be expected experimentally. Figure 15 shows an off-critical blend (15-85) for a dimensionless shear rate, $\dot{\gamma} t_{\mathrm{ps}} = (2u_w/d) t_{\mathrm{ps}} = 0.58$. Initially, long narrow filaments formed and eventually they broke apart into droplets due to the well-known Taylor-Tomotika instability [106]. The droplets (Fig. 16) then became elongated and tilted at approximately 45° relative to the shear plane, as predicted in the limit of a low concentration of dispersed droplets [108]. However, at a later stage of phase separation (Fig. 17), the droplets coalesce to form undulating string structures that seem to persist indefinitely in a ''dynamic string state'' (a video of our simulation can be found in Ref. [109]). The correlated motions of the strings suggest that the hydrodynamic interactions between the strings and/or between the strings and the boundary of the sheared fluid seem to be playing an important role in the stabilization and formation of the extended string structures. Subsequent experiments have indicated a similar string formation phenomenon in an off-critical blend sheared at low shear rates in a parallel plate geometry having a narrow gap relative to the droplet size [110].

### C. Surface-directed phase separation

As a final illustrative application of the LB method, we consider an example of blend phase separation where one boundary is solid and the other interface is fluid (Figs. 18–21). Figure 18 shows the initial fluid composition at a quench depth of $\tau_G = 0.7$. The dark liquid phase has a preferential interaction [111] with both the solid substrate (bottom boundary) and a third fluid (''air''). This image illustrates the well known phenomena of ''surface-directed spinodal decomposition,'' in which the compositional waves of phase separation are brought into registry with the symmetry-breaking walls [95,112–116]. The coarsening of the layer structure at early and intermediate times occurs much like a bulk blend (see Fig. 12), but the continued coarsening at long times requires the intermittent loss of fluid layers. At some point, the undulations within the layers grow sufficiently large (perhaps associated with the rupture of inner layers as required by coarsening) to induce perforations in the outer surface of the blend film at the polymer-air boundary (Fig. 20). This undulation phenomenon then causes the layered structure to break up into a structure that superficially resembles a spinodal decomposition pattern when seen from above (Fig. 21). A number of studies have indicated the presence of a ''fast mode'' [117] in layered blend films, corresponding to a rapidly growing length scale con-

sistent with a hydrodynamic instability. The instability shown in Figs. 18–21 provides a possible explanation for the geometrical nature of this transition. Further computational and experimental studies of the late-stage coarsening instabilities in layered blends would clearly be interesting to check this novel picture of phase separation in thin quiescent films in which the surface exerts a strong perturbing influence on the phase-separating blend film structure.

## VII. CONCLUSIONS

The development of the lattice Boltzmann methods of simulating flows in multiphase liquids has developed rapidly in recent years. The time has come to evaluate the critical phenomena that characterize basic thermodynamic and hydrodynamic properties of this type of model. We performed numerical experiments on a LB fluid model to determine the equilibrium critical properties that are most important for comparison with real fluids. The results of those simulations are represented in a reduced variable description that is largely independent of the particulars of the model facilitating comparisons with other models of fluid mixtures and with experiment. This type of representation should also be advantageous in expressing experimental measurements in a model-independent form. Our observations indicate that the critical properties (coexistence curves, correlation length, interfacial profile, surface tension) of the LB fluid correspond to an ideal mean-field fluid over a broad range of temperatures. This makes comparisons of the model to experiment particularly appropriate to the high molecular weight polymer blends and other fluid mixtures (perhaps also including some ionic fluids and fluid mixtures containing dissolved salts [90,91]) that can be reasonably modeled by mean-field theory.

Now that we have established the equilibrium critical properties of LB fluid mixtures, we are in a position to study much more complicated problems involving fluid flow, phase separation, and interacting complex boundaries. We illustrated this type of problem in the case of phase separation in critical and off-critical fluid mixtures with and without shear. We also considered the perturbing influence of boundaries on quiescent phase separation and the flow instabilities that can occur in late stages of phase separation.

Our bulk blend phase-separation studies show that the morphology of the phase-separation process in its early and intermediate stages depends on the fluid composition. The early stage of phase separation corresponds to the growth of the local composition to the value of the coexisting composition. Coarsening proceeds at a later stage. The phase-separation morphology had a bicontinuous form under off-critical conditions and the minority phase had a droplet morphology in a far off-critical blend. Previous LB calculations have emphasized the kinetics of phase separation, which is not the emphasized phenomena here [11,98–100]. In future work, we plan to study the crossover between the droplet to bicontinuous phase-separation morphology as a function of viscosity mismatch, composition, and quench depth.

Next, we considered the more challenging problem of phase separation under steady shear. Again we considered on- and off-critical blends and found the morphologies to be qualitatively different. Shear had the effect of causing the phase-separation morphology to ''streak'' into a stringlike morphology near the boundary of the critical composition phase-separating blend, leading to a complex gradient structure within the blend. The ''penetration'' depth of the surface-induced strings seemed to grow with time in the course of phase separation. The ultimate configuration of the phase-separated blend, alignment parallel or perpendicular to the flow direction, depends on the polymer surface interaction. These observations of fluid heterogeneity on intermediate time scales clearly raise questions about the proper interpretation of light scattering and optical microscopy studies of blends under shear, since these methods often involve an averaging over the gradient structure or are limited to observations of the near-surface properties of the mixture, respectively. The off-critical sheared blend simulations revealed a tendency toward droplet distortion and tilted alignment with respect to the shear flow direction. At a latter stage, we observed droplet alignment and the droplets subsequently coalescenced into a stringlike morphology. These strings seem to be very stable under shear, which we expect to arise from the strong hydrodynamic interactions between the strings and the shearing boundaries in these highly confined phase-separating fluids (see Fig. 17). A similar phenomenon in off-critical blends sheared at low rates in a confined geometry has recently been observed experimentally [110].

In our final illustrative example, we considered the perturbing influence of solid and air boundaries on the phase separation of a blend. The existence of a ''free'' deformable boundary (polymer-air interface) makes this a particularly instructive example of some of the advantages of the LB method. We observe the development of composition waves in the phase-separating blend, as observed in many previous experimental and simulation studies with a preferential interaction between one of the blend components and the boundaries [110,112–116]. The simulation illustrates the process by which layers are lost in the course of phase coarsening. These film coarsening processes apparently lead to a destabilization of the layer structure in a late stage of phase separation. The fluctuations within the film associated with successive film rupture processes cause the layer structure to collapse like a disturbed ''house of cards,'' leading to a polymer blend morphology *superficially* resembling a bicontinuous ''spinodal'' pattern. These observations emphasize the importance of time-dependent studies of blend film morphologies in measurements on real blend films to properly interpret their origin.

Our illustrations of LB calculations of blend phase separation were purposely restricted to relatively simple geometries and flows that are under current study for their potential relevance to processing applications. It is also possible to incorporate many other fluid properties of interest (shear dependence of fluid viscosity) and other important effects (temperature gradients and time-dependent temperature variations, density mismatch of fluid components and segregation with gravitational and centrifugal fields, fluid wetting and dewetting on heterogeneous substrates, phase separation of

blend films on patterned substrates, phase separation in electric fields, phase separation at high rates of flow where inertial effects are important, flow in complex geometries and with the presence of filler inclusions, etc.). There are many possibilities for further application. An important challenge for future theoretical work is the incorporation of fluctuation effects to better describe fluid properties near the critical point for phase separation.

## ACKNOWLEDGMENTS

The authors would like to acknowledge useful conversations with Hudong Chen and Xiayio He. We thank Newell Washburn for his constructive remarks related to phase separation in asymmetric fluid mixtures. We also appreciate the assistance of John Hagedorn and Terry Griffin of the Information and Technology Laboratory at the National Institute of Standards and Technology in the flow visualization. N.S.M. would like to acknowledge partial support from the National Institute of Standards and Technology Center for Theoretical and Computational Materials Science.

## APPENDIX A: CONTRIBUTION TO PRESSURE TENSOR FROM FLUID/FLUID INTERACTION

Here it is useful to discuss the relation between the LB model and other mean-field models of phase separation. First, consider the equation for a single-particle distribution function $P_1$ based on the continuum BBGKY [8,9] formalism, which is extended to the case of multiple species,

$$\partial_t P_1^i + \vec{k}_1 \cdot \nabla P_1^i + \vec{F} \cdot \nabla_k P_1^i = \Omega^i, \tag{A1}$$

where $\vec{k}$ is the microscopic momentum, $F$ is the acceleration due to a body force, and $\Omega$ is a collision operator. It can be shown, when making a molecular chaos approximation [9], that the collision operator can be written as

$$\Omega^i = -\sum_{j=1}^{s} \frac{\partial P_1^i(\vec{r}_1, \vec{k}_1, t)}{m \partial \vec{k}_1} \times \int d^3 r_2 \rho^j(\vec{r}_2, t) g_{ij}(\vec{r}_1, \vec{r}_2, t) \frac{\partial V_{ij}(r_{12})}{\partial \vec{r}_1}. \tag{A2}$$

This approximation of the collision operator is of the form of a body-force term, $F \cdot \nabla_k P_1$. For $|\vec{r}_1 - \vec{r}_2| > d$, where $d$ is of order a few ''effective'' hard-sphere diameters, $g_{ij}(\vec{r}_1, \vec{r}_2) \approx 1$. After expanding $\rho^j$ about $r_1$, the contribution to the collision operator associated with the attractive intermolecular interaction, $\Omega^i$ can be approximated by $\Omega^i = \Sigma_{j=1}^{s} \nabla V_m^{ij} \cdot \nabla_k P_1^i$, where $V_m^{ij} = 2a_{ij}\rho^j(\vec{r}_1) + \kappa_{ij} \nabla^2 \rho^j(\vec{r}_1)$ with $a_{ij} = \frac{1}{2}\int_d d^3 r V_{ij}(r)$ and $\kappa_{ij} = \frac{1}{6}\int_d d^3 r\, r^2 V_{ij}(r)$. $V_m^{ij}$ can be thought of as a mean-field potential produced by neighboring particles and $-\nabla V_m^{ij}$ is the associated mean-field force.

The pressure tensor can be determined for this system,

$$\begin{aligned} \overleftrightarrow{P} = [ & -a_{11}\ \rho_1^2 - a_{22}\ \rho_2^2 - 2a_{12}\ \rho_1\rho_2 \\ & + \kappa_{11}(\tfrac{1}{2}|\nabla\rho_1|^2 + \rho_1\nabla^2\rho_1) + \kappa_{22}(\tfrac{1}{2}|\nabla\rho_2|^2 + \rho_2\nabla^2\rho_2) \\ & + \kappa_{12}(\nabla\rho_1\cdot\nabla\rho_2 + \rho_1\nabla^2\rho_2 + \rho_2\nabla^2\rho_1)]\overleftrightarrow{I} - \kappa_{11}\nabla\rho_1\nabla\rho_1 \\ & - \kappa_{22}\nabla\rho_2\nabla\rho_2 - 2\kappa_{12}(\nabla\rho_1\nabla\rho_2 + \nabla\rho_2\nabla\rho_1). \end{aligned}$$

This expansion is a counterpart of the Cahn-Hilliard or Landau free-energy expansion [12,17]. The forcing used in this paper is for the case in which all terms in the above pressure tensor are zero except that with the coefficient $a_{12}$, which is proportional to the coupling constant, $G$, described earlier in the paper. While there is no explicit inclusion of a surface tension term in the model studied in this paper, an effective surface tension force results in the Shan-Chen model due to how the forcing between fluid components is incorporated. This can be seen from the leading term in the expansion of $F$,

$$F \sim \rho(x + \Delta x) - \rho(x - \Delta x) \approx \frac{\partial \rho}{\partial x}, \tag{A3}$$

where $F^2$ corrections to the pressure tensor, a feature in the Shan-Chen model [7], scale with the surface tension as in standard Cahn-Hilliard models. Higher-order terms, from Chapman-Enskog analysis, also contribute to the effective surface tension, along with contributions that arise from finite-difference approximations of the contiuum equations. Quantitative predictions of the surface tension require an understanding of all these terms.

## APPENDIX B: HARD-SPHERE CORRECTION TO INTERACTION TERM

The usual lattice Boltzmann method assumes that the fluid is composed of point particles. To include a volume exclusion interaction and in effect obtain a relative volume of the fluid particles, we utilize an Enskog hard-sphere model. The relative volume fraction can be determined from the sphere radius and the number density. The application of Enskog theory to multicomponent fluid mixtures is described by López de Haro *et al.* [118] and in references cited in this work. While there are different formulations of hard-sphere models, such as standard Enskog theory (SET) and revised Enskog theory (RET), we will utilize a form of forcing, arising from hard-sphere interactions that are treated to lowest order in density. In this case, the two theories are identical. Further details are described in Ref. [118]. In the isothermal regime, the additional correction to the forcing due to hard-sphere collisions, $B^{i(\mathrm{HS})}$, is

$$B_a^{i(\mathrm{HS})} = -\frac{2b_{ij}\chi_{ijc}}{n^j} n_a^{i(\mathrm{eq})}(\mathbf{e_a}-\mathbf{v})\cdot\frac{\partial n^j}{\partial \mathbf{x}}, \qquad \text{(B1)}$$

where $\chi_{ijc}$ is the equilibrium value of the pair correlation function for spheres of species $i$ and $j$ at contact with the equilibrium density replaced by the total local equilibrium density at the point $\mathbf{x}$, $b_{ij}=\frac{2}{3}\pi n_j\sigma_{ij}^3/\rho$, with $\sigma_{ij}$ equal to the distance between sphere centers in contact and $\rho$ is the local density. The total forcing on a fluid component $i$ is then $B_a^i + B_a^{i(\mathrm{HS})}$, where $B_a^i$ is defined in Eq. (13).


[1] For a review of applications of lattice Boltzmann and lattice gas methods, see S. Chen and G. Doolen, Annu. Rev. Fluid Mech. **30**, 329 (1998); D. H. Rothman and S. Zaleski, Rev. Mod. Phys. **66**, 1417 (1994).

[2] X. Shan and H. Chen, Phys. Rev. E **47**, 1815 (1992); **49**, 2941 (1994).

[3] M. R. Swift, W. R. Osborn, and J. M. Yeomans, Phys. Rev. Lett. **75**, 830 (1995); W. R. Osborn, E. Orlandini, M. R. Swift, J. M. Yeomans, and J. R. Banavar, *ibid.* **75**, 4031 (1995).

[4] A. K. Gunstensen, D. H. Rothman, S. Zaleski, and G. Zanetti, Phys. Rev. A **43**, 4320 (1991); A. K. Gunstensen, Ph.D. thesis, MIT, 1992; A. K. Gunstensen and D. H. Rothman, Europhys. Lett. **18**, 157 (1992).

[5] N. S. Martys and H. Chen, Phys. Rev. E **53**, 743 (1996).

[6] F. M. Auzerais, J. Dunsmuir, B. B. Ferréol, N. Martys, J. Olson, T. S. Ramakrishnan, D. H. Rothman, and L. M. Schwartz, J. Geophys. Res. B **23**, 705 (1996).

[7] N. S. Martys, X. Shan, and H. Chen, Phys. Rev. E **58**, 6855 (1998).

[8] S. Chapman and T. G. Cowling, *The Mathematical Theory of Non-Uniform Gases*, 3rd ed. (Cambridge University Press, London, 1970). BBGKY is an abbreviation for Bogoliubov, Born, Green, Kirkwood, and Yvon.

[9] R. L. Liboff, *Kinetic Theory*, 2nd ed. (John Wiley & Sons, New York, 1998).

[10] N. S. Martys, Int. J. Mod. Phys. C **10**, 1367 (1999).

[11] J. W. Cahn and J. E. Hilliard, J. Chem. Phys. **28**, 258 (1958); **31**, 688 (1959).

[12] J. W. Cahn, Trans. Metall. Soc. AIME **242**, 166 (1968).

[13] A. J. Bray, Adv. Phys. **43**, 357 (1994).

[14] J. D. Gunton, M. Miguel, and P. S. Sahni, *Phase Transitions and Critical Phenomena*, edited by C. Domb and J. L. Lebowicz (Academic Press, New York, 1983), Vol. 9.

[15] S. C. Glotzer, Annu. Rev. Comput. Phys. **2**, 1 (1995).

[16] E. Orlandini, M. R. Swift, and J. M. Yeomans, Europhys. Lett. **32**, 463 (1995).

[17] H. E. Stanley, *Introduction to Phase Transitions and Critical Phenomena* (Oxford University Press, New York, 1971).

[18] R. J. Baxter, *Exactly Solved Models in Statistical Mechanics* (Academic Press, New York, 1982).

[19] A. R. Miller, *The Theory of Solutions of High Polymers* (Clarendon Press, Oxford, 1948).

[20] J. H. Hildebrand and R. L. Scott, *The Solubility of Non-Electrolytes* (Reinhold, New York, 1950).

[21] P. J. Flory, *Principles of Polymer Chemistry* (Cornell University Press, Ithaca, New York, 1953); P. G. de Gennes, *Scaling Concepts in Polymer Science* (Cornell University Press, Ithaca, 1979).

[22] K. F. Freed and J. Dudowicz, Theor. Chim. Acta **82**, 357 (1992).

[23] Y. H. Qian, D. d'Humières, and P. Lallemand, Europhys. Lett. **17**, 479 (1992).

[24] H. Chen, S. Y. Chen, and W. H. Matthaeus, Phys. Rev. A **45**, R5339 (1992).

[25] X. Shan and G. Doolen, Phys. Rev. E **54**, 3614 (1996).

[26] R. Perl and R. A. Ferrel, Phys. Rev. A **6**, 2358 (1972); R. A. Ferrel, Phys. Rev. Lett. **24**, 1169 (1970); see also J. F. Douglas, Macromolecules **25**, 1468 (1992).

[27] K. Kawasaki, Ann. Phys. (N.Y.) **61**, 1 (1970).

[28] O. Onuki and K. Kawasaki, Ann. Phys. (N.Y.) **121**, 456 (1979).

[29] O. Onuki, K. Yamazaki, and K. Kawasaki, Ann. Phys. (N.Y.) **131**, 217 (1981).

[30] J. V. Sengers, Int. J. Thermophys. **6**, 203 (1985); H. C. Burstyn and J. V. Sengers, Phys. Rev. Lett. **45**, 259 (1980); Phys. Rev. A **25**, 448 (1982).

[31] P. Stepanek, T. P. Lodge, C. Kedrowski, and F. S. Bater, J. Chem. Phys. **94**, 8289 (1991).

[32] J. C. Nieuwoudt and J. V. Sengers, J. Chem. Phys. **90**, 457 (1989).

[33] J. Dudowicz, M. Lifschitz, K. F. Freed, and J. F. Douglas, J. Chem. Phys. **99**, 4804 (1993); M. Lifschitz, J. Dudowicz, and K. F. Freed, *ibid.* **100**, 3957 (1994).

[34] A. Sariban and K. Binder, J. Chem. Phys. **86**, 5859 (1987).

[35] D. A. McQuarrie, *Statistical Mechanics* (Harper and Row, New York, 1976).

[36] D. C. Mattis, *Theory of Magnetism* (Harper and Row, New York, 1985).

[37] T. Lee and C. Yang, Phys. Rev. **87**, 410 (1952).

[38] N. D. Mermin and J. J. Rehr, Phys. Rev. A **4**, 2408 (1971); N. D. Mermin, Phys. Rev. Lett. **26**, 169 (1971).

[39] B. Widom and J. Rowlinson, J. Chem. Phys. **52**, 1670 (1970).

[40] J. A. Zollweg and G. W. Mulholland, J. Chem. Phys. **57**, 1021 (1972).

[41] G. Stell and P. C. Hemmer, J. Chem. Phys. **56**, 4274 (1972).

[42] J. V. Sengers, in *Supercritical Fluids: Fundamentals for Applications*, edited by E. Kiran and J. M. H. Levelt Sengers (Kluwer, Dordrecht, 1994), pp. 231–271.

[43] V. L. Ginzburg, Fiz. Tverd. Tela (Leningrad) **2**, 2031 (1960) [Sov. Phys. Solid State **2**, 1824 (1960)].

[44] M. A. Anisimov, S. B. Kiselev, J. V. Sengers, and S. Tan, Physica A **188**, 487 (1992).

[45] P. G. de Gennes, J. Phys. (France) Lett. **38**, L441 (1977).

[46] K. Binder, J. Chem. Phys. **79**, 6378 (1983); Phys. Rev. A **29**, 341 (1984).

[47] F. S. Bates, J. Rosedale, P. Stepanek, T. P. Lodge, P. Wiltzius, G. H. Fredrickson, and R. P. Hjelm, Phys. Rev. Lett. **65**, 1893 (1990).

[48] E. K. Hobbie, L. Reed, C. C. Huang, and C. C. Han, Phys. Rev. E **48**, 1579 (1993).
[49] D. Schwahn, T. Schmackers, and M. Mortensen, Phys. Rev. E **52**, R1288 (1995).
[50] J. H. M. Levelt Sengers and J.V. Sengers, *Perspectives in Statistical Physics*, edited by H. J. Raveché (North Holland Publ. Co., New York, 1981).
[51] S. V. Kazakov and N. I. Chernnova, Russ. J. Phys. Chem. **69**, 1010 (1995).
[52] A. A. Povodyrev, M. A. Anisimov, and J. V. Sengers, Physica A **264**, 345 (1999).
[53] I. C. Sanchez, J. Phys. Chem. **93**, 6983 (1989); P. Damay and F. Leclercq, J. Chem. Phys. **95**, 590 (1991).
[54] L. Cailletet and E. C. Mathias, C. R. Hebd. Seances Acad. Sci. **102**, 1202 (1886); **104**, 1563 (1887); E. A. Guggenheim, J. Chem. Phys. **13**, 253 (1945).
[55] J. W. Yu, J. F. Douglas, E. K. Hobbie, S. Kim, and C. C. Han, Phys. Rev. Lett. **78**, 2664 (1997).
[56] M. W. Pestak, R. R. Goldstein, M. H. W. Chan, J. R. de Bruyn, D. A. Balzarini, and N. W. Ashcroft, Phys. Rev. B **35**, 599 (1987); J. S. Rowlinson, Nature (London) **319**, 362 (1985).
[57] D. Blankschtein, G. M. Thurston, and G. B. Benedek, Phys. Rev. Lett. **54**, 995 (1985); X.-H. Guo and S.-H. Chen, *ibid.* **64**, 1979 (1990).
[58] The dissimilarity in molecular size in a fluid mixture can be modeled in a more physically realistic way by including different size parameters for the interacting species in the specification of the collision operator in an Enskog-type model of the particle interaction. See Appendix B and X. He, H. Shan, and G. Doolen, Phys. Rev. E **57**, R13 (1998).
[59] G. H. Gilmer, W. Gilmore, J. Huang, and W. W. Web, Phys. Rev. Lett. **14**, 491 (1965).
[60] D. Beaglehole, Physica B & C **112**, 330 (1982).
[61] D. Beysens and M. Robert, J. Chem. Phys. **87**, 3056 (1987).
[62] D. G. Miles, Jr. and J. W. Schmidt, J. Chem. Phys. **92**, 3881 (1990).
[63] J. W. Schmidt, Physica A **172**, 40 (1991).
[64] J. W. Schmidt and M. R. Moldover, J. Chem. Phys. **99**, 582 (1993).
[65] A. Karim, G. P. Felcher, and T. P. Russel, Macromolecules **27**, 6973 (1994).
[66] T. Karle, J. Klein, and K. Binder, Phys. Rev. Lett. **77**, 1318 (1998).
[67] F. P. Buff, R. A. Lovett, and F. H. Stillinger, Phys. Rev. Lett. **15**, 621 (1965).
[68] J. V. Sengers, J. M. J. Van Leeuwen, and J. W. Schmidt, Physica A **172**, 20 (1991).
[69] A. Werner, F. Schmid, M. Müller, and K. Binder, J. Chem. Phys. **107**, 8175 (1997).
[70] M. Müller, K. Binder, and W. Oed, J. Chem. Soc., Faraday Trans. **91**, 2369 (1995).
[71] J. D. van der Waals, Z. Phys. Chem., Stoechiom. Verwandtschaftsl. **13**, 657 (1894).
[72] S. Fisk and B. Widom, J. Chem. Phys. **50**, 3219 (1969).
[73] P. Debye, J. Chem. Phys. **31**, 680 (1959).
[74] K. Binder, Adv. Polym. Sci. **112**, 181 (1994).
[75] P. Chieux, J.-F. Jal, L. Hily, J. Dupuy, P. Leclercq, and P. Damay, J. Phys. IV **C-5**, 3 (1991).
[76] V. G. Vaks, A. I. Larkin, and S. A. Pikin, Zh. Éksp. Teor. Fiz. **51**, 361 (1966) [Sov. Phys. JETP **24**, 240 (1967)].
[77] M. R. Moldover, Phys. Rev. A **31**, 1022 (1985).
[78] H. Chaar, M. R. Moldover, and J. W. Schmidt, J. Chem. Phys. **85**, 418 (1986); B. Widom, J. Stat. Phys. **52**, 1343 (1988); I. Szleifer and B. Widom, J. Chem. Phys. **90**, 7524 (1989).
[79] I. Szleifer, J. Chem. Phys. **92**, 6940 (1990).
[80] The coexistence curve for $\delta_M \neq 1$ is actually fairly symmetric in volume fraction units.
[81] A. Karim, Ph.D. thesis, Northwestern University, 1990 (unpublished).
[82] R. L. Sammler, R. P. Dion, C. J. Carriere, and A. Cohen, Rheol. Acta **31**, 554 (1992).
[83] S. H. Anastasiadis, I. Gencarz, and J. T. Koberstin, Macromolecules **21**, 2980 (1988).
[84] D. Atack and O. K. Rice, Discuss. Faraday Soc. **15**, 210 (1953). See Ref. [1] for a discussion of these data.
[85] A. Stammer and B. A. Wolf, Polymer **39**, 2065 (1998).
[86] M. Heinrich and B. A. Wolf, Polymer **33**, 1927 (1992).
[87] B. Widom, J. Chem. Phys. **43**, 3892 (1965).
[88] J. F. Douglas, Macromolecules **25**, 1468 (1992).
[89] H. P. Deutsch and K. Binder, J. Phys. II **3**, 1049 (1993); M. Müller and K. Binder, Macromolecules **28**, 1825 (1995).
[90] J. Jacob, A. Kumar, M. A. Anisimov, A. A. Povodyrev, and J. V. Sengers, Phys. Rev. E **58**, 2188 (1998); B. M. Jaffer Ali and A. Kumar, Phys. Lett. A **237**, 257 (1998).
[91] K. S. Pitzer, M. Conceicao, P. de Lima, and D. R. Schreiber, J. Chem. Phys. **89**, 1854 (1985); D. R. Schreiber, M. Conceicao, P. de Lima, and K. S. Pitzer, *ibid.* **91**, 4087 (1987); R. R. Singh and K. S. Pitzer, *ibid.* **92**, 6775 (1990).
[92] A. Sariban, K. Binder, and D. W. Heerman, Phys. Rev. B **35**, 6873 (1987).
[93] Y. C. Chou and W. I. Golburg, Phys. Rev. A **23**, 2105 (1979).
[94] M. Takenaka, T. Izumitani, and T. Hashimoto, Macromolecules **20**, 2257 (1987).
[95] B. P. Lee, J. F. Douglas, and S. C. Glotzer, Phys. Rev. E **60**, 5812 (1999).
[96] L. P. McMaster, Adv. Chem. Ser. **142**, 43 (1975); E. D. Siggia, Phys. Rev. A **20**, 595 (1970).
[97] S. Chen and T. Lookman, J. Stat. Phys. **81**, 223 (1995).
[98] M. R. Swift, E. Orlandini, W. R. Osborn, and J. M. Yeomans, Phys. Rev. E **54**, 5041 (1996).
[99] J. Olson and D. H. Rothman, J. Stat. Phys. **81**, 199 (1995).
[100] F. J. Alexander, S. Chen, and D. W. Grunau, Phys. Rev. B **48**, 634 (1993).
[101] F. Perrot, P. Guenoun, T. Baumberg, D. Beysens, Y. Garrabos, and B. LeNeindre, Phys. Rev. Lett. **73**, 688 (1994).
[102] I. S. Miles and A. Zurek, Polym. Eng. Sci. **28**, 1796 (1988); G. M. Jordhamoo, J. A. Manson, and L. H. Sperling, *ibid.* **26**, 517 (1986).
[103] T. Hashimoto, K. Matsuzaka, E. Moses, and A. Onuku, Phys. Rev. Lett. **74**, 126 (1995); E. Moses, T. Kume, and T. Hashimoto, *ibid.* **72**, 2037 (1994); E. K. Hobbie, S. Kim, and C. C. Han, Phys. Rev. E **54**, 5909 (1996); S. Kim, E. K. Hobbie, J. Yu, and C. C. Han, Macromolecules **30**, 8245 (1997).
[104] A. H. Krall, J. V. Sengers, and K. Hamano, Phys. Rev. Lett. **69**, 1963 (1992).

[105] A. J. Wagner and J. M. Yeomans, Phys. Rev. E **59**, 4366 (1999).
[106] G. I. Taylor, Proc. R. Soc. London, Ser. A **138**, 41 (1932); S. Tomotika, *ibid.* **150**, 322 (1935).
[107] M. San Miguel, M. Grant, and J. D. Gunton, Phys. Rev. A **31**, 1001 (1985); L. Sung, A. Karim, J. F. Douglas, and C. C. Han, Phys. Rev. Lett. **76**, 4368 (1996).
[108] J. M. Rallison, J. Fluid Mech. **209**, 465 (1981); H. A. Stone, Annu. Rev. Fluid Mech. **26**, 65 (1994).
[109] http://www.itl.nist.gov/div895/savg/example/index.html.
[110] K. B. Migler, Phys. Rev. Lett. (to be published).
[111] The incorporation of component-specific surface interactions in multicomponent fluids requires a modification to the equilibrium distribution to maintain its positive-definite property. This technical point will be discussed in a separate publication.
[112] R. A. L. Jones, L. J. Norton, E. J. Kramer, F. S. Bates, and P. Wiltzius, Phys. Rev. Lett. **66**, 1326 (1991).
[113] G. Krausch, C. A. Dai, E. J. Kramer, and F. Bates, Phys. Rev. Lett. **71**, 3669 (1993).
[114] R. C. Ball and R. L. H. Essery, J. Phys.: Condens. Matter **2**, 10 303 (1990).
[115] S. Puri and K. Binder, Phys. Rev. A **46**, R4487 (1992); Phys. Rev. E **49**, 5359 (1993).
[116] J. F. Marko, Phys. Rev. E **48**, 2861 (1993).
[117] P. Wiltzius and A. Cumming, Phys. Rev. Lett. **66**, 3000 (1991); C. Harrison, W. Rippard, and A. Cumming, Phys. Rev. E **52**, 723 (1995).
[118] M. López de Haro, E. G. D. Cohen, and J. M. Kincaid, J. Chem. Phys. **78**, 2746 (1983).